Available online at www.sciencedirect.com

ScienceDirect

Geochimica et Cosmochimica Acta 221 (2018) 182–199

Geochimica et Cosmochimica Acta

www.elsevier.com/locate/gca

NanoSIMS isotope studies of rare types of presolar silicon carbide grains from the Murchison meteorite: Implications for supernova models and the role of ^{14}C

Peter Hoppe [a,*], Marco Pignatari [b,c], János Kodolányi [a], Elmar Gröner [a], Sachiko Amari [d]

[a] Max Planck Institute for Chemistry, Hahn-Meitner-Weg 1, 55128 Mainz, Germany
[b] E.A. Milne Centre for Astrophysics, University of Hull, Hull HU6 7RX, UK
[c] NuGrid Collaboration[1]
[d] McDonnell Center for the Space Sciences and the Physics Department, Washington University, St. Louis, MO 63130, USA

Received 26 August 2016; accepted in revised form 25 January 2017; available online 9 February 2017

Abstract

We have conducted a NanoSIMS ion imaging survey of about 1800 presolar silicon carbide (SiC) grains from the Murchison meteorite. A total of 21 supernova (SN) X grains, two SN C grains, and two putative nova grains were identified. Six particularly interesting grains, two X and C grains each and the two putative nova grains were subsequently studied in greater detail, namely, for C-, N-, Mg-Al-, Si-, S-, and Ca-Ti-isotopic compositions and for the initial presence of radioactive ^{26}Al (half life 716,000 yr), ^{32}Si (half life 153 yr), and ^{44}Ti (half life 60 yr). Their isotope data along with those of three X grains from the literature were compared with model predictions for 15 $M_\odot$ and 25 $M_\odot$ Type II supernovae (SNe). The best fits were found for 25 $M_\odot$ SN models that consider for the He shell the temperature and density of a 15 $M_\odot$ SN and ingestion of H into the He shell before the explosion. In these models a C- and Si-rich zone forms at the bottom of the He burning zone (C/Si zone). The region above the C/Si zone is termed the O/nova zone and exhibits the isotopic fingerprints of explosive H burning. Satisfactory fits of measured C-, N-, and Si-isotopic compositions and of $^{26}Al/^{27}Al$ ratios require small-scale mixing of matter originating from a region extending over 0.2 $M_\odot$ for X and C grains and over 0.4 $M_\odot$ for one of the putative nova grains, involving matter from a thin Si-rich layer slightly below the C/Si zone, the C/Si zone, and the O/nova zone. Simultaneous fitting of $^{14}N/^{15}N$ and $^{26}Al/^{27}Al$ requires a C-N fractionation of a factor of 50 during SiC condensation. This leads to preferential incorporation of radioactive ^{14}C (half life 5700 yr) over directly produced ^{14}N and can account for the $^{14}N/^{15}N$ along with $^{26}Al/^{27}Al$ ratios as observed in the SiC grains. The good fit for one of the putative nova grains along with its high $^{26}Al/^{27}Al$ points towards a SN origin and supports previous suggestions that some grains classified as nova grains might be from SNe. Apparent problems with the small-scale mixing scheme considered here are C/O ratios that are mostly <1 if C-, N-, and Si-isotopic compositions and $^{26}Al/^{27}Al$ ratios are simultaneously matched, underproduction of ^{32}Si, and overproduction of ^{44}Ti. This confirms the limitations of one-dimensional hydrodynamical models for H ingestion and stresses the need to better study the convective-boundary mixing mechanisms at the bottom of the convective He shell in massive star progenitors. This is crucial to define the effective size of the C/Si zone formed by the SN shock. The comparison between the Si isotope data of the SN grains and the models gives a hint that the predicted ^{30}Si is too high at the bottom of the He burning shell.

Keywords: Meteorites; Presolar grains; Silicon carbide; Supernovae; Secondary ion mass spectrometry

* Corresponding author.
E-mail address: peter.hoppe@mpic.de (P. Hoppe).
[1] http://www.nugridstars.org

http://dx.doi.org/10.1016/j.gca.2017.01.051
0016-7037/

1. INTRODUCTION

Primitive meteorites, interplanetary dust particles, and matter returned from comet Wild 2 contain small quantities (up to several 100 ppm) of refractory dust grains that formed in the winds of evolved stars and in the ejecta of stellar explosions (Zinner, 2014). These grains are older than our Solar System and are known as "presolar grains". These pristine samples can be distinguished from matter that formed or was processed in the early Solar System by large isotopic abundance anomalies in major and minor elements. After their discovery in the late 1980s it was quickly realized that presolar grains represent samples of stardust that can be studied in the laboratory in great detail. Among the presolar minerals identified to date are nanodiamonds (Lewis et al., 1987), silicon carbide (SiC) (Bernatowicz et al., 1987; Tang and Anders, 1988), graphite (Amari et al., 1990), silicon nitride (Si_3N_4) (Nittler et al., 1995), oxides, e.g., corundum and other forms of Al_2O_3 and spinel (Hutcheon et al., 1994; Nittler et al., 1994), and silicates (Messenger et al., 2003). With the exception of the nanodiamonds, whose origin is still a matter of debate, presolar grains have typical sizes of several 100 nm, and a small fraction of them have sizes even in the micrometer-range.

Laboratory studies of individual presolar grains can provide information on stellar nucleosynthesis and evolution, mixing in supernova (SN) ejecta, Galactic chemical evolution, grain formation in stellar environments, processing of dust in the interstellar medium, the types of stars that contributed dust to our Solar System, and materials processing in early Solar System history. Thousands of individual presolar grains have been studied by secondary ion mass spectrometry (SIMS) for isotopic compositions. A key SIMS instrument for isotope studies of the light and intermediate-mass elements in presolar grains is the NanoSIMS ion probe (Hoppe et al., 2013). This secondary ion mass spectrometer permits isotope and elemental abundance measurements with spatial resolution down to 50 nm for Cs^+ primary ions and down to 200 nm for O^- primary ions. Important complementary analysis techniques are resonance ionization mass spectrometry (RIMS) for isotope analyses of intermediate-mass and heavy elements (e.g., Nicolussi et al., 1997; Stephan et al., 2016) and transmission electron microscopy for mineralogical studies of electron-transparent sections prepared by microtomy or focused ion beam technique (Croat et al., 2003; Zega et al., 2007; Holzapfel et al., 2009).

Silicon carbide is by far the best characterized presolar mineral. This is because (i) it can be separated from meteorites by physical and chemical treatments in almost pure form, (ii) it is relatively abundant, and (iii) it has relatively high concentrations of elements other than C and Si. Based on the isotopic compositions of C, N, and Si presolar SiC is divided into seven distinct populations (Zinner, 2014): Mainstream (MS), AB, C, X, Y, Z, and nova grains. Most abundant are the MS grains which constitute up to about 90% of all grains. MS grains formed in the winds of 1.5–3 $M_\odot$ asymptotic giant branch (AGB) stars of about solar metallicity[2] (Lugaro et al., 2003; Zinner et al., 2006). Important arguments in favor of such stars are the C-isotopic ratios as well as the imprints of slow neutron capture (s-process) nucleosynthesis in the isotopic patterns of heavy elements in MS grains. The Type Y and Z grains (a few percent of all known SiC grains) are thought to come from low-mass AGB stars of sub-solar metallicities as concluded from their C and Si isotope ratios (Hoppe et al., 1997; Amari et al., 2001b). The Type AB grains constitute a few percent of SiC and are characterized by $^{12}C/^{13}C < 10$ (Amari et al., 2001c). Their origin is still a matter of debate and among the proposed stellar sources are J-type carbon stars (Lambert et al., 1986) and born-again AGB stars, such as Sakurai's object (Asplund et al., 1999), but some AB grains might also be from supernovae (SNe) and novae (Liu et al., 2016). A small group of grains has $^{12}C/^{13}C < 10$ along with low $^{14}N/^{15}N$ ratios (<40) and these grains are likely from novae (Amari et al., 2001a) and/or SNe (Nittler and Hoppe, 2005; Liu et al., 2016). The rare Type X (~1% of all SiC) and C (~0.1% of all SiC grains) formed in the ejecta of Type II SN (SNII) explosions. The X and C grains can be distinguished by their Si-isotopic ratios: X grains exhibit strong enrichments in ^{28}Si, whereas the C grains show large enrichments in the heavy Si isotopes. Other important characteristics of SiC from SNe are super-solar $^{12}C/^{13}C$ ratios (most grains) and sub-solar $^{14}N/^{15}N$ ratios, and, inferred from large isotopic overabundances of ^{26}Mg, ^{32}S (especially in the C grains), ^{44}Ca, and ^{49}Ti, incorporation of high abundances of radioactive ^{26}Al (half-life 716,000 yr), ^{32}Si (half life 153 yr), ^{44}Ti (half-life 60 yr), and ^{49}V (half life 330 d) at the time of grain formation (Nittler et al., 1996; Hoppe and Besmehn, 2002; Hoppe et al., 2000, 2010, 2012; Lin et al., 2010; Pignatari et al., 2013b; Xu et al., 2015). X grains were subdivided into sub-groups, based on $^{29}Si/^{30}Si$ ratios (X0, X1, and X2 grains; Lin et al., 2010), and C grains according to $^{12}C/^{13}C > 10$ or $^{12}C/^{13}C < 10$ (C1 and C2 grains; Liu et al., 2016). Note that the grain labels used in this work do not refer to these sub-groups.

Here, we report on a NanoSIMS C and Si ion imaging survey of about 1800 submicrometer-sized SiC grains from the Murchison separates KJA and KJD (median sizes of 0.38 μm and 0.81 μm, respectively; Amari et al., 1994), conducted to search for grains with extreme isotopic compositions. Five particularly interesting grains (one C grain with very high $^{12}C/^{13}C$, two X grains with very low $^{29}Si/^{30}Si$, and two putative nova grains) were subsequently studied for N, Mg-Al, S, and Ca-Ti isotopic compositions. Their isotope data along with those of four SiC SN grains from the literature (one typical X grain, two X grains with very low $^{29}Si/^{30}Si$, one typical C grain for which a complementary N isotope measurement was conducted here) will be discussed in the context of the SNII models of Rauscher et al. (2002) and Pignatari et al. (2013a, 2015). The model by Rauscher et al. (2002) has been successfully used to account, at least qualitatively, for the isotopic signatures of many C and X grains (Hoppe et al., 2010, 2012; Lin

[2] Metallicity is the mass fraction of elements heavier than He.

et al., 2010). In the context of this model significant Si contributions come from inner SN zones while the other major element C comes mostly from outer SN zones. The intermediate zones are O-rich and contributions from these zones must be strongly limited in the ejecta where SiC forms, to have C/O > 1, a necessary condition for SiC formation under equilibrium conditions (Lodders and Fegley, 1995). The concept of selective, large-scale mixing in SN ejecta is not without problems and has been the subject of a lively debate. Recently, Pignatari et al. (2013a, 2015) have presented new SN models with comparatively high explosion energies of 3–5 × 10^{51} erg, in which a C- and Si-rich zone forms at the bottom of the He-burning shell, an attractive site for SiC formation, which does not require the selective, large-scale mixing anymore. While in these one-dimensional models explosion energy has a large impact on the nucleosynthesis signatures obtained at the bottom of the He shell (e.g., through its influence on the maximum temperature attained), it is important to note that in realistic asymmetric core-collapse SN explosions many components, corresponding to different explosion energies, may be present (e.g., Nomoto et al., 2013; Müller, 2016). The isotope ratios of the nine presolar SiC grains considered here exhibit wide ranges of isotopic compositions and we will use them to test the validity of the Pignatari et al. models and to provide new constraints to develop these models further.

2. EXPERIMENTAL

2.1. Samples

Thousands of SiC grains from Murchison separates KJA and KJD (Amari et al., 1994) were transferred in an isopropanol suspension to clean gold foils. Prior to the isotope studies both mounts were scanned with low magnification in the Leo 1530 FE-SEM at the Max Planck Institute for Chemistry to search for regions with grain densities suitable for automated NanoSIMS ion imaging.

2.2. Ion imaging

Systematic C and Si isotope measurements were done on the KJA and KJD mounts by the fully automated ion imaging procedure developed for the Cameca NanoSIMS 50 ion probe at the Max Planck Institute for Chemistry (Gröner and Hoppe, 2006). Prior to ion imaging the analyzed areas were cleaned and implanted with Cs by pre-sputtering with a high-current Cs^+ ion beam for about 30 min (~100 pA beam current, 0.0035 pA/μm^2). The ion imaging procedure consists of three steps: (i) Acquisition of negative secondary ion images of ^{12}C, ^{13}C, ^{28}Si, ^{29}Si, and ^{30}Si, produced by rastering (256 × 256 pixels, 15,000 μs/pixel) a focused primary Cs^+ beam (~1 pA, 100 nm size, 16 keV energy) over 30 × 30 μm^2-sized areas in a multi-collection mode. (ii) Identification of SiC grains based on the ^{28}Si ion image and acquisition of ion images with sizes of two times the grain size (defined at the 10% of the maximum ^{28}Si intensity) with an integration time of 60 s. (iii) Movement of the sample stage to an adjacent area and repetition of steps (i) to (iii). In this way a total of 202 (KJA) and 143 (KJD) areas were analyzed on which ~1170 (KJA) and ~640 (KJD) SiC grains were identified. Measured C- and Si-isotopic compositions were normalized to those measured on our in-house synthetic, fine-grained N-doped SiC standard ($\delta^{13}C_{PDB}$[3] = −29.1 ± 1.2‰, assumed $\delta^{29,30}Si = 0$‰ relative to the terrestrial composition; hereafter all uncertainties are 1σ).

2.3. Isotope measurements on selected SiC grains

Two X grains from the KJA mount, and one C grain and two putative nova grains from the KJD mount (Fig. 1) were subsequently measured for N (all grains), Mg-Al (all grains except one KJA grain), S (all grains), and Ca-Ti isotope (all KJD grains) compositions. For the KJA grains we recorded in multi-collection negative secondary ions of ^{12}C, $^{12}C^{14}N$, $^{12}C^{15}N$, ^{32}S, and ^{34}S (session 1), employing a Cs^+ primary ion beam (~1 pA beam current, 100 nm beam diameter, rastered over 1.5 × 1.5 – 2 × 2 μm^2) and positive secondary ions of ^{24}Mg, ^{25}Mg, ^{26}Mg, ^{27}Al, and ^{28}Si (session 2), employing an O^- primary ion beam (~5 pA, 400 nm, 3 × 3 μm^2). For the KJD grains we recorded in multi-collection negative secondary ions of ^{12}C, ^{13}C, $^{12}C^{14}N$, $^{12}C^{15}N$, and ^{28}Si (session 1), and of ^{28}Si, ^{32}S, ^{33}S, ^{34}S, and ^{36}S (session 2), employing a Cs^+ primary ion beam (~1 pA, 100 nm, 2 × 2 μm^2), and positive secondary ions of ^{24}Mg, ^{25}Mg, ^{26}Mg, ^{27}Al, and ^{28}Si (session 3) and of ^{28}Si, ^{40}Ca, ^{42}Ca, ^{44}Ca, and ^{48}Ti (session 4), employing an O^- primary ion beam (~5 pA, 400 nm, 2 × 2 – 3 × 3 μm^2). In addition, one previously studied grain (M7-D, Fig. 1; Hoppe et al., 2012) was measured for its N-isotopic composition in a setup identical to session 1 of the KJD analyses.

To correct for instrumental mass fractionation and differences in the electron multiplier detection efficiencies, measured isotopic ratios were normalized to those measured on the same SiC standard as that used for ion imaging (N and S; the standard is doped with N and it contains S in sufficiently high quantities for use as a standard), on Burma Spinel (Mg-Al), and on terrestrial perovskite (Ca-Ti). In general, large excesses in ^{26}Mg, ^{32}S, and ^{44}Ca can be attributed to the decay of radioactive ^{26}Al, ^{32}Si, and ^{44}Ti, respectively. Inferred initial $^{26}Al/^{27}Al$ ratios presented here were calculated from $^{26}Al/^{27}Al = \delta^{26}Mg/1000 \times (^{26}Mg/^{24}Mg)_\odot/(^{27}Al^+/^{24}Mg^+) \times \varepsilon(Al^+)/\varepsilon(Mg^+)$ or, if Mg is monoisotopic ^{26}Mg from $^{26}Mg^+/^{27}Al^+ \times \varepsilon(Al^+)/\varepsilon(Mg^+)$. The relative sensitivity factor $\varepsilon(Al^+)/\varepsilon(Mg^+) = 1.56$ was taken from Hoppe et al. (2010). Similarly, inferred $^{44}Ti/^{48}Ti$ ratios (only upper limits, see section 3.2) were calculated from $^{44}Ti/^{48}Ti = \delta^{40}Ca/1000 \times (^{44}Ca/^{40}Ca)_\odot/(^{48}Ti^+/^{40}Ca^+) \times \varepsilon(Ti^+)/\varepsilon(Ca^+)$. The relative sensitivity factor $\varepsilon(Ti^+)/\varepsilon(Ca^+) = 0.51$ was taken from Besmehn and Hoppe (2003). Following Pignatari et al. (2013b), initial $^{32}Si/^{28}Si$ ratios were calculated from $^{32}Si/^{28}Si = -0.001 \times \delta S \times {}^{32}S^-/{}^{28}Si^- \times \varepsilon(Si^-)/\varepsilon(S^-)$ where δS is the weighted average of $\delta^{33}S$ and $\delta^{34}S$ and $\varepsilon(Si^-)/\varepsilon(S^-) = 1/3$ (Hoppe et al., 2012).

[3] $\delta^xA = [(^xA/^yA)_{Sample}/(^xA/^yA)_{Ref} - 1] \times 1000$, where ^xA is a minor isotope of element A, ^yA the major (or reference) isotope; $(^xA/^yA)_{Ref}$ is the isotopic ratio of a reference standard.

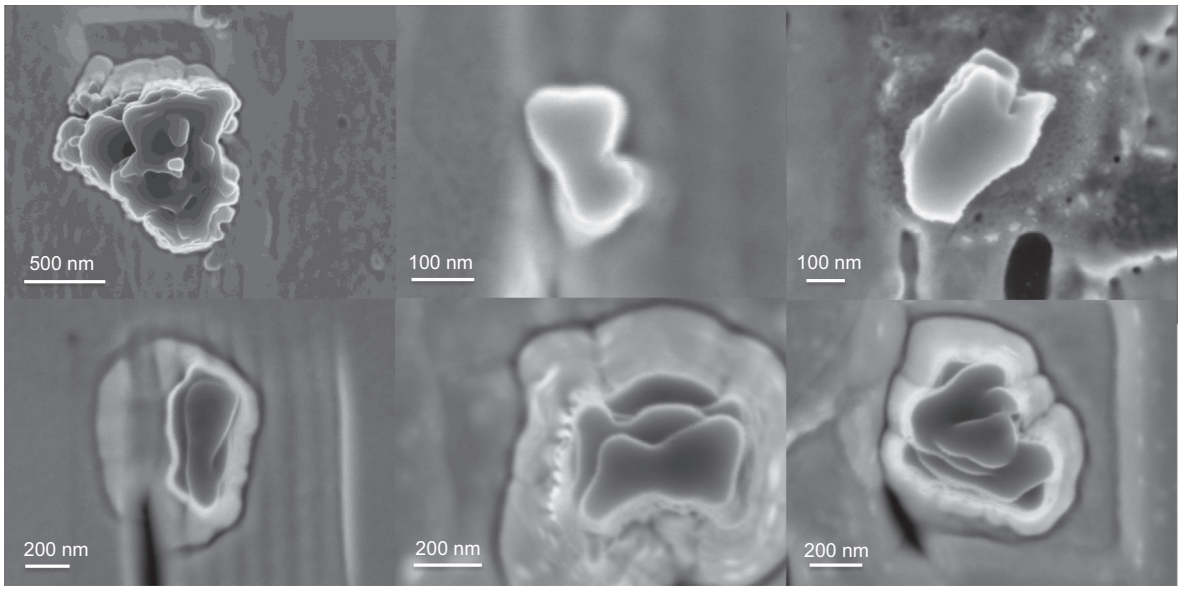

Fig. 1. SEM pictures of six presolar SiC grains from this study after ion imaging in the NanoSIMS. Upper row, from left to right: M7-D (C1), KJA-12-17-15 (X4), KJA-16-19-1 (X5); lower row, from left to right: KJD-6-24-3 (C2), KJD-1-11-5 (N1), KJD-3-23-5 (N2).

3. RESULTS

3.1. SiC populations

To classify the SiC grains from this study we have used the classification scheme of Hoppe et al. (2010), except for the nova grains, for which we use here $^{12}C/^{13}C < 10$ and $^{14}N/^{15}N < 60$. We note, however, that the nova-origin of grains classified as nova grains was questioned (Nittler and Hoppe, 2005; Liu et al., 2016) and we come back to this issue below. A definition of C grains was not given in Hoppe et al. (2010) and we define them here as having $\delta^{29}Si$ and $\delta^{30}Si > 200‰$. The number of identified grains of the different SiC populations and corresponding abundances are given in Table 1. Taking KJA and KJD grains together we find an abundance of ~84% for the most abundant group, the MS grains, which is compatible with what was reported before for submicrometer-sized grains (Zinner et al., 2007; Hoppe et al., 2010; Xu et al., 2015); the same holds for the abundances of the minor SiC populations. Besides SiC grains we also identified two grains with very low C/Si, most likely Si_3N_4 grains, with X grain signature in Si. The SN X and C grains and the putative nova grains together constitute 1.5% of all SiC and Si_3N_4 grains in this study. A total of 23 SiC X and C grains were found. Twelve of them have $^{12}C/^{13}C < 100$, which is compatible with the findings for submicrometer-sized grains in previous studies (Hoppe et al., 2010; Xu et al., 2015). Seven of the X grains from separate KJD were selected for isotope studies with CHILI, a new RIMS instrument at the University of Chicago (Stephan et al., 2016), all of which could be successfully measured for Fe-Ni isotopic compositions (Kodolányi et al., 2018).

For the major elements C and Si we find $^{12}C/^{13}C$ ratios between 1.4 and 21,400 and $\delta^{29}Si$ values from −680‰ to 940‰ and $\delta^{30}Si$ values from −790‰ to 840‰, and up to $\delta^{29}Si = 1080‰$ and $\delta^{30}Si = 1210‰$ if grain C1 (see Table 2; Si data already reported in Hoppe et al., 2012) is considered. The $^{12}C/^{13}C$ ratio of 1.4 of grain N2 (Table 2) is among the lowest $^{12}C/^{13}C$ ratios measured for presolar

Table 1
SiC and Si_3N_4 populations for KJA and KJD grains from this study.

Grain Type	No. of Grains (KJA)	Abundance (%)	No. of Grains (KJD)	Abundance (%)	No. of Grains (KJA + KJD)	Abundance (%)
MS	1017	86.7	494	78.2	1511	83.7
AB	40	3.4	43	6.8	83	4.6
Y	31	2.6	49	7.8	80	4.4
Z	28	2.4	28	4.4	56	3.1
U	44	3.8	5	0.8	49	2.7
X	13	1.1	8	1.3	21	1.2
C	0	0.0	2	0.3	2	0.1
Nova	0	0.0	2	0.3	2	0.1
Si_3N_4-X	1	0.1	1	0.2	2	0.1

Total abundances of 100.1% for KJA and KJD grains are due to rounding errors.

Table 2
Isotopic compositions of selected presolar SiC grains of supernova and putative nova origin.

Grain	Label	Type	Ref.	$^{12}C/^{13}C$	$^{14}N/^{15}N$	$^{26}Al/^{27}Al$	$\delta^{29}Si$ (‰)	$\delta^{30}Si$ (‰)	$\delta^{33}S$ (‰)	$\delta^{34}S$ (‰)	$^{32}Si/^{28}Si$ (10^{-4})	$^{44}Ti/^{48}Ti$
KJE-a2-28-7	X1	X	[1]	693 ± 9	124 ± 5	0.119 ± 0.004	−382 ± 5	−553 ± 4	−144 ± 39	−72 ± 17	6.4 ± 2.0	0.118 ± 0.036
M9–132-4	X2	X	[2]	823 ± 18	44 ± 1	n.m.	−658 ± 5	−234 ± 10	n.m.	n.m.	n.m.	0.248 ± 0.016
287	X3	X	[3]	137 ± 2	116 ± 4	n.m.	−606 ± 4	−195 ± 7	n.m.	n.m.	n.m.	n.m.
KJA-12-17-15	X4	X	This work	222 ± 18	50 ± 2	n.m.	−558 ± 20	−52 ± 37	n.m.	106 ± 228	*<170*[2]	n.m.
KJA-16-19-1	X5	X	This work	2105 ± 421	175 ± 24	*<0.15*[2]	−530 ± 15	−76 ± 28	n.m.	−87 ± 100	*<16*[2]	n.m.
M7-D	C1	C	[4], this work	109 ± 2	147 ± 10	0.122 ± 0.012	1082 ± 12	1207 ± 16	−609 ± 61	−478 ± 142	12.0 ± 2.0	0.077 ± 0.002
KJD-6-24-3	C2	C	This work	21,400 ± 3500	15.0 ± 0.3	*<0.054*[2]	380 ± 15	835 ± 22	−289 ± 178	−185 ± 82	5.6 ± 2.0	*<0.12*[2]
KJD-1-11-5	N1	Nova?	This work	3.7 ± 0.0	57 ± 1	0.205 ± 0.012	−23 ± 9	136 ± 11	−303 ± 110	−94 ± 54	8.1 ± 2.9	*<0.0086*[2]
KJD-3-23-5	N2	Nova?	This work	1.4 ± 0.0	42 ± 1	0.018 ± 0.002	132 ± 15	248 ± 20	−121 ± 141	15 ± 65	*<2.2*[2]	*<0.0012*[2]

[1]: Xu et al. (2015), [2]: Besmehn and Hoppe (2003), [3]: Marhas et al. (2008), [4]: Hoppe et al. (2012).
[2] 2σ upper limit.
n.m.: not measured.

grains to date; similarly low ratios were previously reported by Haenecour et al. (2016), Hoppe et al. (2012), and Liu et al. (2016). The $^{12}C/^{13}C$ ratio of grain C2, on the other hand, is the highest $^{12}C/^{13}C$ ratio ever found for presolar grains.

3.2. Isotopic compositions of selected grains

The C-, N-, Si-, and S-isotopic compositions as well as inferred $^{26}Al/^{27}Al$, $^{32}Si/^{28}Si$, and $^{44}Ti/^{48}Ti$ ratios of six selected grains (two X grains, two C grains, two putative nova grains) from this study are listed in Table 2 (grains with labels X4, X5, C1, C2, N1, N2) and displayed in Fig. 2 (Si), 3 (C and N), 4 (Al and C), and 5 (S). Note that for grain C1 all isotope data, except those for N, were already reported in Hoppe et al. (2012). Grains X4 and X5 were selected for in-depth studies after ion imaging because they have particularly low $^{29}Si/^{30}Si$ ratios (relative to other X grains), grain C1 because it represents a typical C grain, grain C2 because of its very high $^{12}C/^{13}C$ ratio, and grains N1 and N2 because they permit to explore the potential SN origin of grains classified as nova grains.

Grain X4 (240 × 120 nm²): Grain X4 has a very low $^{29}Si/^{30}Si$ of 0.47 times the solar ratio, with a $^{30}Si/^{28}Si$ ratio close to solar (Fig. 2). There are only 3 other grains with comparably low $^{29}Si/^{30}Si$ ratios for which C, Si, and N isotope data exist, two from the literature (grains X2 and X3 in Table 2) and grain X5 from this study. Carbon- and

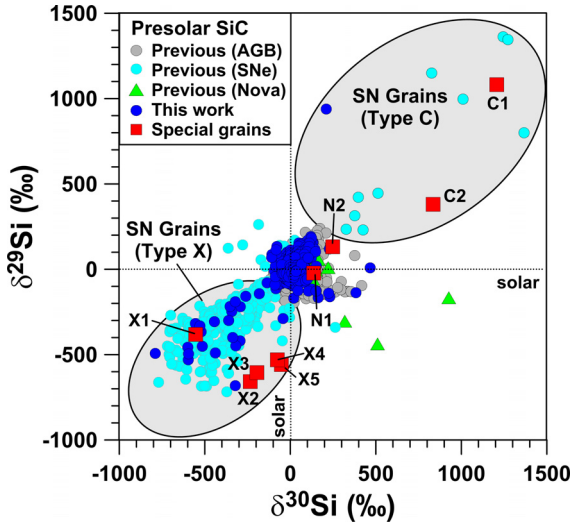

Fig. 2. Silicon-isotopic compositions of presolar SiC grains from ion imaging (this study) and from previous studies. $^{29}Si/^{28}Si$ and $^{30}Si/^{28}Si$ ratios are given as permil deviation from the Solar System ratios. The nine SN and putative nova grains discussed in this work are marked in red. Data from previous studies are from Alexander (1993), Hoppe et al. (1994, 1996, 2000, 2010, 2012), Nittler (1996), Huss et al. (1997), Amari et al. (2001a,c), Lin et al. (2002), Besmehn and Hoppe (2003), Nittler and Alexander (2003), Nittler and Hoppe (2005), Marhas et al. (2008), Xu et al. (2015), Liu et al. (2016). For the literature data only data points with an error of ≤20‰ in $\delta^{30}Si$ are shown. (For interpretation of the references to colour in this figure legend, the reader is referred to the web version of this article.)

N-isotopic ratios ($^{12}C/^{13}C = 222 \pm 18$, $^{14}N/^{15}N = 50 \pm 2$) represent typical ratios for X grains (Fig. 3). Sulfur was strongly affected by contamination and the inferred high upper limit on $^{32}Si/^{28}Si$ has only limited significance.

Grain X5 (420 × 250 nm²): The $^{29}Si/^{30}Si$ ratio of 0.51 times the solar ratio is similarly low as those of grains X2, X3, and X4 (Fig. 2). With its relatively high $^{12}C/^{13}C$ and $^{14}N/^{15}N$ ratios of 2100 ± 400 and 175 ± 24, respectively, it plots above the general trend seen for X and C grains in Fig. 3. Aluminum abundances are very low. This permitted to infer only a 2σ upper limit on $^{26}Al/^{27}Al$ (0.15) which plots within the range observed for X and C grains (Fig. 4). Sulfur-32 is slightly, although not significantly, enriched; a 2σ upper limit on $^{32}Si/^{28}Si$ of 1.6×10^{-3} can be inferred.

Grain C1 (1100 × 900 nm²): This grain can be considered a typical C grain, as is evident from Figs. 2–5. It is the only grain from this study for which we found excess ^{44}Ca ($^{44}Ca/^{40}Ca$ is 19x the solar ratio) along with a solar $^{42}Ca/^{40}Ca$ (Hoppe et al., 2012). The inferred $^{44}Ti/^{48}Ti$ ratio of 0.077 ± 0.002 falls well within the range observed for other X and C grains (Nittler et al., 1996; Hoppe et al., 2000; Besmehn and Hoppe, 2003; Lin et al., 2010; Xu et al., 2015).

Grain C2 (600 × 250 nm²): Grain C2 has not only an extremely high $^{12}C/^{13}C$ ratio of $21{,}400 \pm 3500$ but also a very low $^{14}N/^{15}N$ ratio of 15.0 ± 0.3 which is among the lowest ratios observed for X and C grains (Fig. 3). Its ^{30}Si enrichment is higher than that of ^{29}Si (Fig. 2). The ^{32}S excess of ~20% (Fig. 5) corresponds to $^{32}Si/^{28}Si = (5.6 \pm 2.0) \times 10^{-4}$. Magnesium, Al, Ca, and Ti concentrations are low and no evidence for significant amounts of ^{26}Al and ^{44}Ti was found. The 2σ upper limit on $^{26}Al/^{27}Al$

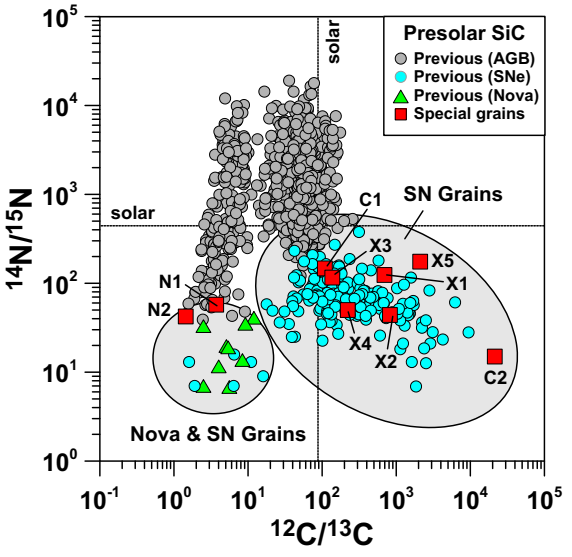

Fig. 3. Carbon and N-isotopic compositions of presolar grains of nine SN and putative nova grains discussed in this work (marked in red) and from previous studies. Data from previous studies are from Hoppe et al. (1994, 1996, 2000, 2010), Nittler (1996), Huss et al. (1997), Amari et al. (2001a,c), Lin et al. (2002), Besmehn and Hoppe (2003), Nittler and Hoppe (2005), Marhas et al. (2008), Xu et al. (2015), Liu et al. (2016). The Solar System ratios are shown by the dotted lines. (For interpretation of the references to colour in this figure legend, the reader is referred to the web version of this article.)

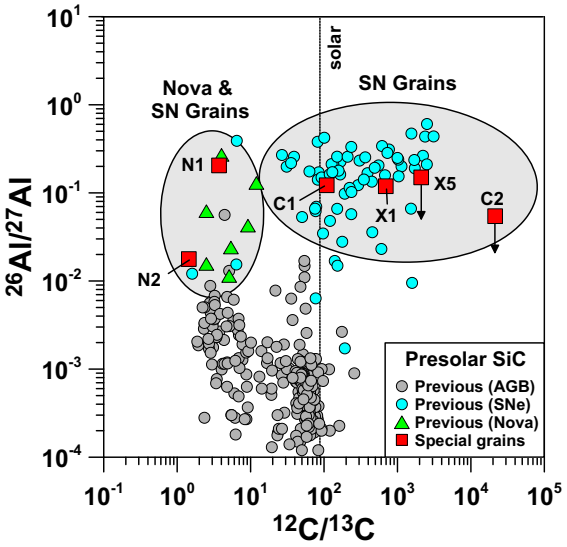

Fig. 4. $^{26}Al/^{27}Al$ and $^{12}C/^{13}C$ ratios of presolar grains of nine SN and putative nova grains discussed in this work (marked in red) and from previous studies. Data from previous studies are from Hoppe et al. (1994, 2000, 2010, 2012), Nittler (1996), Huss et al. (1997), Amari et al. (2001a,c), Lin et al. (2002), Nittler and Hoppe (2005), Xu et al. (2015), Liu et al. (2016). The Solar System $^{12}C/^{13}C$ ratio is shown by the dotted line. (For interpretation of the references to colour in this figure legend, the reader is referred to the web version of this article.)

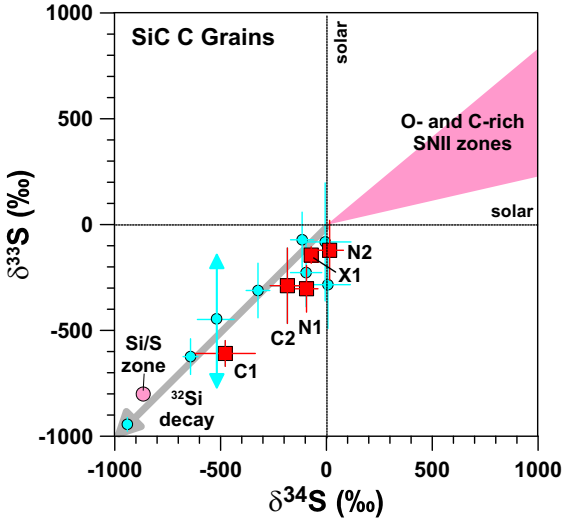

Fig. 5. Sulfur-isotopic compositions of five SN and putative nova grains discussed in this work (marked in red) and of SiC C grains from the literature (Gyngard et al., 2010; Hoppe et al., 2010, 2012; Xu et al., 2015). $^{33}S/^{32}S$ and $^{34}S/^{32}S$ ratios are given as permil deviation from the Solar System ratios. Predictions for the Si/S and O- and C-rich zones in a 15 $M_\odot$ SNII (Rauscher et al., 2002) are shown for comparison. (For interpretation of the references to colour in this figure legend, the reader is referred to the web version of this article.)

of 0.054 plots at the lower end of what is typically observed for X and C grains (Fig. 4); for $^{44}Ti/^{48}Ti$ the 2σ upper limit is relatively high (0.12) and thus not very diagnostic.

Grain N1 (500 × 360 nm²): Grain N1 has $^{12}C/^{13}C = 3.7 \pm 0.1$, $^{14}N/^{15}N = 57.4 \pm 1.3$, $\delta^{29}Si = -23 \pm 9‰$ and $\delta^{30}Si = 136 \pm 11‰$. The C- and Si-isotopic compositions are compatible with previously found nova grains while its $^{14}N/^{15}N$ ratio plots at the upper end of previously observed values (Figs. 2 and 3). Magnesium is monoisotopic ^{26}Mg with $^{26}Al/^{27}Al = 0.205 \pm 0.012$ (Fig. 4), which is higher than for other putative nova grains, except for one grain, whose nova origin, however, was questioned (Nittler and Hoppe, 2005). Grain N1 exhibits a small but significant ^{32}S excess (Fig. 5) from which $^{32}Si/^{28}Si = (8.1 \pm 2.9) \times 10^{-4}$ can be inferred. No evidence for ^{44}Ti was found, albeit large uncertainties exist; the 2σ upper limit calculates to 0.0086.

Grain N2 (520 × 360 nm²): Grain N2 has $^{12}C/^{13}C = 1.4 \pm 0.1$, $^{14}N/^{15}N = 42.3 \pm 0.5$, $\delta^{29}Si = 132 \pm 15‰$ and $\delta^{30}Si = 248 \pm 20‰$ (Figs. 2 and 3). As for grain N1, its $^{14}N/^{15}N$ ratio is higher than that of most other nova grains. Magnesium is essentially monoisotopic ^{26}Mg with $^{26}Al/^{27}Al = 0.018 \pm 0.002$, as similarly observed for typical nova grains (Fig. 4). No evidence for ^{32}S and ^{44}Ti was found with 2σ upper limits of 2.2×10^{-4} for $^{32}Si/^{28}Si$ and of 1.2×10^{-3} for $^{44}Ti/^{48}Ti$.

4. DISCUSSION

There is general consensus that X and C grains originate from SNe, based on their specific isotopic signatures (see, e.g., Zinner, 2014, and references therein). We will thus not discuss other potential stellar sources and focus on SNe. As the nova origin of grains classified as nova grains was questioned (Nittler and Hoppe, 2005; Liu et al., 2016) we will include two grains from this study (N1, N2) classified as nova grains in the discussion and explore whether they could have a SN origin. In the following discussion we will compare the isotope data of the six presolar grains from this study with predictions from the SNII models of Rauscher et al. (2002) and Pignatari et al. (2013a, 2015). We will also include three additional grains from the literature, two X grains with low $^{29}Si/^{30}Si$ (Besmehn and Hoppe, 2003; Marhas et al., 2008) for which C, N, and Si isotope data exist, and of a typical X grain for which the full set of isotope data considered here is available (Xu et al., 2015). Section 4.1 gives brief descriptions of the SN models. In Section 4.2 we present comparisons between the grain data and the model predictions. In a first step we search for the best fits for the isotopic compositions of the major elements C and Si and the most abundant minor element N, which is found up to the percent level in SiC SN grains. In a second step we judge the fit quality for the abundances of the radioactive nuclides ^{26}Al, ^{32}Si, and ^{44}Ti and make adjustments to the fits, if possible. Finally, in Section 4.2.3 we discuss the constraints from the SN grain data and identify shortcomings in the current Pignatari models, which demonstrates the need to produce a new generation of massive star models, guided from multi-dimensional hydrodynamics simulations.

4.1. Supernova models

All stars heavier than about 8–10 $M_\odot$ are believed to explode as core-collapse SNe (e.g., Jones et al., 2013). Rauscher et al. (2002) have presented yields of several hundred isotopes throughout the ejecta after passage of the shock wave but prior to mixing in the ejecta for SNeII with masses from 15 to 25 $M_\odot$. These models assume an initial solar composition and use a range of experimental and theoretical nuclear data. Before the explosion a SNII consists of concentric layers that experienced different stages of nuclear burning. Following the nomenclature of Meyer et al. (1995) we name these layers according to the most abundant elements present (Fig. 6). These layers experienced partial H burning (H zone), H burning (He/N), H and partial He burning (He/C), He burning (O/C), C burning (O/Ne), Ne and partial O burning (O/Si), O burning (Si/S), and explosive Si burning and an α-rich freezeout from nuclear statistical equilibrium (Ni). Profiles of ^{12}C, ^{14}N, ^{16}O, and ^{28}Si are displayed in Fig. 6. For our comparisons of grain data with predictions from the SN models of Rauscher et al. (2002) we considered the 15 $M_\odot$ model with standard nuclear physics, namely, model s15a28c (available on www.nucleosynthesis.org). We integrated the abundances of all isotopes in each of the zones and determined fractions of each zone required to best match the grains' isotope data. This large-scale, selective mixing approach follows previously applied schemes which were able to get satisfactory matches for many presolar grains of presum-

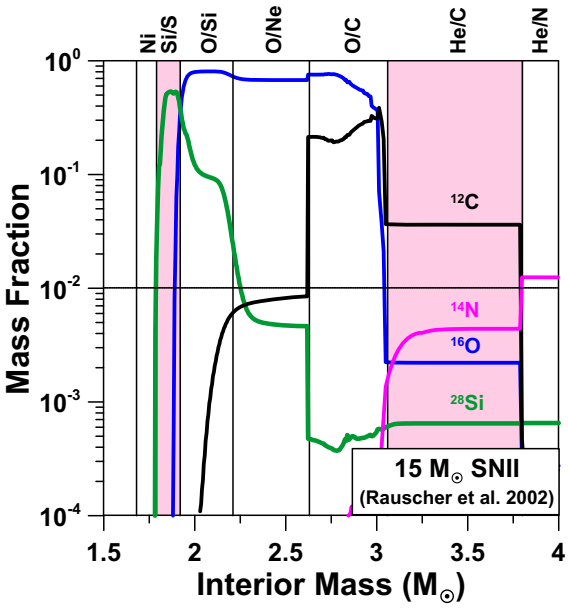

Fig. 6. Profiles of mass fractions of ^{12}C, ^{14}N, ^{16}O, and ^{28}Si in the interior of a 15 $M_\odot$ SNII according to model s15a28c of Rauscher et al. (2002). The SN is divided into 8 distinct layers that experienced different stages of nuclear burning. The layers are named according to the most abundant elements (at the top), following the nomenclature given in Meyer et al. (1995). The Si- and C-rich and O-poor zones are marked in pink. (For interpretation of the references to colour in this figure legend, the reader is referred to the web version of this article.)

ably SN origin (e.g., Nittler et al., 2008; Hoppe et al., 2010; Lin et al., 2010; Xu et al., 2015). It should be noted, however, that some unsolved problems exist when the population of SN grains is evaluated as a whole, such as matching the highest $^{26}Al/^{27}Al$ ratios, the connection of $^{26}Al/^{27}Al$ with $^{12}C/^{13}C$ ratios, and the general trend of Si isotope ratios of X grains which can be qualitatively accounted for, but not quantitatively. Models generally predict lower $^{26}Al/^{27}Al$ for higher $^{12}C/^{13}C$, a pattern which is not seen in the data of SN grains (e.g., Lin et al., 2010; Xu et al., 2015). Furthermore, it was pointed out by Lin et al. (2010) that the models would have to produce a primary component in which ^{28}Si is accompanied by ^{29}Si with a ratio $^{29}Si/^{28}Si \sim 0.024$ which is not evident from current SN models. More recently, Pignatari et al. (2013a) have presented a new set of SNII models. These models consider a 15 $M_\odot$ progenitor star of solar metallicity and three different shock velocities following the explosion. The explosion simulations include the fallback prescription by Fryer et al. (2012), resulting in high shock velocities and high temperatures during explosive He burning. These shock velocities correspond to explosion energies of up to $3–5 \times 10^{51}$ erg. Following observations of SN1987A, explosion energies of 1×10^{51} erg have been considered as a reference for core-collapse SNe in the past (e.g., Woosley and Weaver, 1995; Limongi and Chieffi, 2003). However, there is a large scatter in observed explosion energies for SN progenitor masses up to 25 $M_\odot$, ranging from 0.6 to 6×10^{51} erg (see, e.g., Fig. 2 in Nomoto et al., 2013), well encasing the energies considered here. Moreover, SN explosions are highly asymmetric (Grefenstette et al., 2014) and it is well conceivable that a SN with explosion energy on the order of 1×10^{51} erg exhibits conditions in parts of the He shell that are obtained in one-dimensional SN models for higher explosion energies. These asymmetries may be already present in the pre-SN structure of the massive star progenitor, in particular in the final days before the explosion (see e.g., Müller, 2016 and references therein). While such asymmetries may be crucial for the onset of a successful SN explosion, they may also leave important nucleosynthesis signatures in presolar grains.

At temperatures $>1–1.5 \times 10^9$ K, ^{16}O produced by He burning in the pre-SN phase is partially destroyed during passage of the SN shock, and α-capture reactions will strongly enrich ^{28}Si instead. This leads to a C- and Si-rich and O-poor zone at the bottom of the He/C zone, termed C/Si zone (Fig. 7). This zone represents an attractive source of the material from which SiC condenses at lower T and makes the selective, large-scale mixing required when using the models of Rauscher et al. (2002) in principle redundant, but lacks sufficient ^{13}C and N to account for the signatures of SiC SN grains. In a follow-up work, Pignatari et al. (2015) presented new models in which significant amounts of H are ingested into the He shell of a 25 $M_\odot$ solar metallicity progenitor star prior to the core-collapse SN event. The ingested H is not fully exhausted before the explosion. Due to the passage of the SN shock hot CNO cycle isotopic signatures are predicted above the C/Si zone in a layer termed O/nova zone (Fig. 8). This leads to the production of large amounts of, e.g., ^{13}C, ^{15}N, and ^{26}Al. This new set of

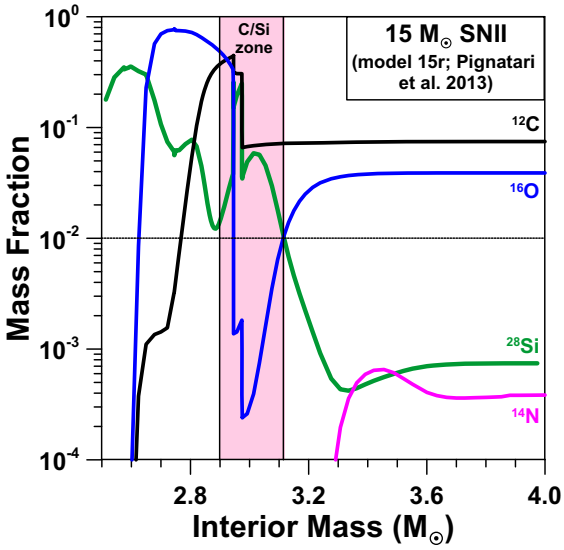

Fig. 7. Profiles of mass fractions of ^{12}C, ^{14}N, ^{16}O, and ^{28}Si in the interior of a 15 $M_\odot$ SNII according to model 15r of Pignatari et al. (2013a). The C- and Si-rich and O-poor zone at the bottom of the He burning zone (C/Si zone) is marked in pink. The limits of the C/Si zone are defined by C and Si mass fractions >1 wt% and by C/O >1 (corresponding to $^{12}C/^{16}O$ mass fractions >0.75). (For interpretation of the references to colour in this figure legend, the reader is referred to the web version of this article.)

models is based on model 25d described in Pignatari et al. (2016). They consider six different concentrations of H in the He shell, with a maximum of 1.2% H. Hydrogen ingestion is predicted to occur only in the 25 $M_\odot$ model but not in the 15 $M_\odot$ model. However, to mimic the conditions of a 15 $M_\odot$ SNII, predicted to have higher temperature and density in the He shell, temperature and density in the He shell were artificially increased in one 25 $M_\odot$ model series accordingly. The models from this series were termed 25T-Hx where x represents the reduction factor of H relative to the maximum amount of 1.2% and has values of 1, 5, 10, 20, 50, and 500, respectively. Here, we will focus on models 25T-H, 25T-H10, 25T-H20, and 25T-H50.

4.2. Grain data vs. model predictions

4.2.1. Rauscher models

The paper of Rauscher et al. (2002) presents yields of isotopes in the ejecta of SNeII in a mass range from 15 $M_\odot$ to 25 $M_\odot$. Here, we will focus mostly on the 15 $M_\odot$ SNII model as previous work has shown that this model provides the most satisfactory fit to SiC X and C grain data among the Rauscher models (Hoppe et al., 2009, 2010), particularly because it generally gives higher C/O and predicts more ^{29}Si than, e.g., the 25 $M_\odot$ SNII model.

In our work presented here, given the observed ranges of C-, N-, and Si-isotopic compositions of X and C grains, we consider a fit of the model data to the SiC grain data as satisfactory when C- and N-isotopic ratios are reproduced within a factor of 2 and $^{29}Si/^{28}Si$ and $^{30}Si/^{28}Si$ ratios within

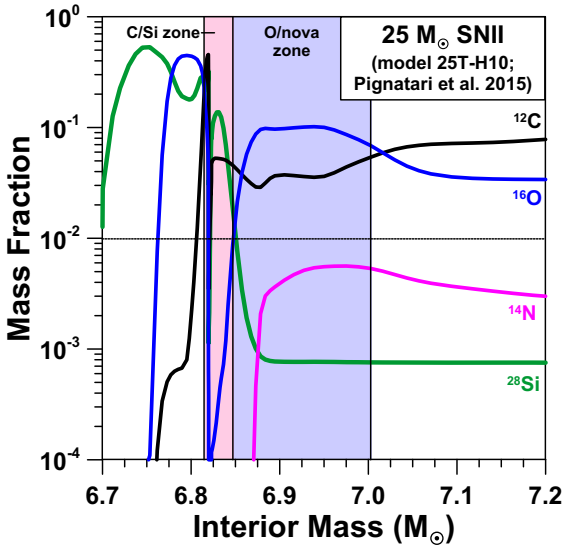

Fig. 8. Profiles of mass fractions of ^{12}C, ^{14}N, ^{16}O, and ^{28}Si in the interior of a 25 $M_\odot$ SNII according to model 25T-H10 of Pignatari et al. (2015). The C- and Si-rich and O-poor zone at the bottom of the He burning zone (C/Si zone) is marked in pink. The limits of the C/Si zone are defined by C and Si mass fractions >1 wt% and by C/O >1 (corresponding to $^{12}C/^{16}O$ mass fractions >0.75). The zone above the C/Si zone exhibits isotopic signatures of explosive H burning and is named O/nova zone (marked in blue). The upper mass limit of this zone is defined by C/O = 1. (For interpretation of the references to colour in this figure legend, the reader is referred to the web version of this article.)

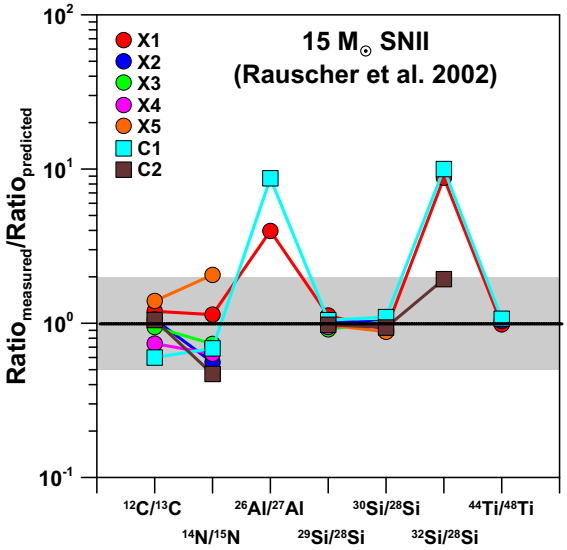

Fig. 9. Measured over predicted isotope ratios for 5 X grains and two C grains. Predictions are from the 15 $M_\odot$ SNII of Rauscher et al. (2002); see text for details. The gray-shaded area indicates a factor of 2 deviation of measured over predicted ratios.

10%. This can be achieved for all X and C grains (Fig. 9) by mixtures that contain different proportions of matter from all 8 SN zones (Table 3). It should be noted, however, that a good fit to the Si isotope data of grains X1, C1, and C2 requires a twofold enhanced ^{29}Si abundance in the O/Si and O/Ne zones as suggested by Hoppe et al. (2009). This is based on an earlier suggestion by Travaglio et al. (1998) who pointed out that SN models may underestimate the yields of ^{29}Si in the C- and Ne-burning zones. On the other hand, for grains X2, X3, X4, and X5, which have particularly low $^{29}Si/^{30}Si$ ratios, a good fit to the Si-isotopic ratios is only achieved without the twofold increase in the ^{29}Si yield in the O/Si and O/Ne zones. This inconsistency may point to shortcomings in the current understanding of the production of the minor Si isotopes in SNeII.

As it can be seen from Fig. 9 also the $^{44}Ti/^{48}Ti$ ratios of X and C grains can be well fitted. But this is not surprising because this ratio can be matched by admixture of matter from the Ni zone which affects the other isotope ratios considered here only marginally. For $^{26}Al/^{27}Al$ the situation is different, as it cannot be independently matched. It is highest in the He/N zone where it is 0.23. However, because in our mixing schemes more than 65% of the matter comes from other zones, the predicted $^{26}Al/^{27}Al$ ratios are much lower (up to 10x) than measured (Fig. 9). Xu et al. (2015) have shown that this problem can be overcome with a SN model of lower mass, namely, the 12 $M_\odot$ SN model of Woosley and Heger (2007) with which the C, N, and Si isotope ratios as well as $^{26}Al/^{27}Al$ and $^{44}Ti/^{48}Ti$ of grain X1

Table 3
Mixing fractions (in percent of total mass in the mixture) of different SN zones in model s15a28c of Rauscher et al. (2002) required to reproduce C and X grain data.

Zone	X1[1]	X2[2]	X3[2]	X4[2]	X5[2]	C1[1]	C2[1]
Ni	0.70	5.0	0.0	0.0	0.0	0.28	0.0
Si/S	0.73	0.98	0.43	0.49	0.64	0.007	0.24
O/Si	0.13	0.90	0.39	0.67	0.88	0.30	0.84
O/Ne	1.1	0.0	0.0	0.0	0.0	0.91	0.42
O/C	7.6	0.0	0.0	0.0	6.7	3.8	21.2
He/C	32.9	58.8	25.7	43.8	57.7	13.0	73.0
He/N	19.4	24.3	15.1	5.2	34.1	7.7	4.3
H	37.4	10.0	58.4	49.8	0.0	74.0	0.0
C/O	0.72	2.98	1.63	2.15	1.04	0.55	0.77
$^{28}Si/^{12}C$	0.05	0.11	0.12	0.09	0.05	0.03	0.015

[1] Model s15a28c from Rauscher et al. (2002) with twofold enhanced ^{29}Si in the O/Si and O/Ne zones according to Hoppe et al. (2009).
[2] Model s15a28c from Rauscher et al. (2002).

can be simultaneously matched. Grain C2 has a comparatively low 2σ upper limit on $^{26}Al/^{27}Al$ of 0.054 which is compatible with the predicted ratio of about 0.02. In our mixing scheme for grain C2 most of the matter (94%) comes from the O/C and He/C zones (Table 3), i.e., experienced He burning. The $^{26}Al/^{27}Al$ ratio of grain C2 confirms the predicted low ^{26}Al production from He burning.

Predicted $^{32}Si/^{28}Si$ ratios are also significantly lower (up to 10x) than inferred for grains X1, C1, and C2. Silicon-32 is a product of n-capture reactions accompanying He burning and the $^{32}Si/^{28}Si$ ratio is highest in the O/C zone with an averaged value of 0.007. In the other He burning zone, the He/C zone, it is only on the order of 10^{-6}. Matter from the O/C zone must be limited as to account for the observed $^{12}C/^{13}C$ ratios and to preserve a reasonably high C/O ratio

which results in the observed mismatch for $^{32}Si/^{28}Si$. We note that in order to have at least some ^{32}Si in the mixtures for grains X1, C1, and C2 (Table 3) inclusion of matter from the O/C zone leads to C/O ratios of lower than 1 (0.55–0.77). A shift of the peak in the ^{32}Si production more towards the He/C zone would relax the observed discrepancy for $^{32}Si/^{28}Si$ and would lift the C/O ratio above unity. We note that the 12 $M_\odot$ SN model of Woosley and Heger (2007) considered by Xu et al. (2015) to account for the isotope data of grain X1 predicts higher $^{32}Si/^{28}Si$ than inferred, just the opposite of what is predicted by the 15 $M_\odot$ Rauscher et al. (2002) model. This demonstrates that the production of certain isotopes is very sensitive to the mass of the progenitor star.

The C-, N-, and Si-isotopic ratios of grains N1 and N2 cannot be simultaneously matched by the Rauscher models. The lowest $^{12}C/^{13}C$ ratio is predicted for the He/N zone with $^{12}C/^{13}C = 3.6$. This would match the C-isotopic ratio of grain N1; however other isotopic ratios, namely, $^{14}N/^{15}N$ and $^{30}Si/^{28}Si$ would not fit, especially $^{14}N/^{15}N$ would be off by three orders of magnitude. Fitting these ratios would increase the $^{12}C/^{13}C$ ratio significantly. The situation is even worse for grain N2 whose $^{12}C/^{13}C$ ratio is lower by a factor of 2.5 than the predicted ratio in the He/N zone.

4.2.2. Pignatari (NuGrid) models

The models of Pignatari et al. (2013a, 2015) are attractive for SiC formation as they predict a C- and Si-rich (C/Si) zone at the bottom of the He burning zone. We define the limits of this zone by ^{12}C and ^{28}Si mass fractions >1 wt% along with C/O > 1. Because C is essentially ^{12}C in the C/Si zone, a result of He burning, it is clear that admixture of ^{13}C-rich matter is necessary to account for the X and C grain data, even for grains with high $^{12}C/^{13}C$ ratios. The 15r model of Pignatari et al. (2013a) predicts a He/N zone with low $^{12}C/^{13}C$ between 4.510 and 4.885 $M_\odot$ (mass coordinate from center) which is similar to the respective zone in the Rauscher models. If we integrate all the matter from the C/Si zone (2.899–3.114 $M_\odot$) up to the He/N zone we find $^{12}C/^{13}C = 9000$. This is still too high for most SiC SN grains and only integration up to 7 $M_\odot$ (i.e., up to the H-rich envelope) brings $^{12}C/^{13}C$ to values typical of SiC SN grains. However, this approach is unsatisfactory because the integration of matter that experiences complete mixing down to the microscopic scale extends over more than 4 $M_\odot$ and because other isotopic ratios, e.g., N and Si, of typical SiC SN grains cannot be matched. Xu et al. (2015) tried to circumvent this in that they selected various sub-layers from the 15r model over ~2 $M_\odot$ which were mixed in variable proportions, with only minor contributions from the C/Si zone.

We will follow a different approach here and focus on the 25T-Hx models of Pignatari et al. (2015). These models provide a source of ^{13}C, ^{15}N, and ^{26}Al close to the C/Si zone. Model 25T-H produces lots of ^{13}C and ^{15}N and will be explored in the context of grain N2. For the other grains we investigated models 25T-H10, 25T-H20, and 25T-H50 in which the He shell contains 0.12%, 0.06%, and 0.024% H, respectively, before the explosion. In these models the C/Si zone is located between 6.8145 and 6.8471 $M_\odot$. The $^{12}C/^{13}C$ ratio in the C/Si zone exhibits the same fundamental problem as in model r15, as it is orders of magnitudes larger than observed in SiC SN grains. The O/nova zone, which extends from 6.8471 to 7.0026 $M_\odot$, provides the missing ^{13}C. We also considered a ^{28}Si- and O-rich rich zone of 0.0145 $M_\odot$ below the C/Si zone, in order to account for the Si-isotopic ratios of X grains. We have subdivided the C/Si zone into two and the O/nova zone into three sub-zones. Together with the Si-rich zone (considered from 6.80 to 6.8145 $M_\odot$) and a zone above the O/nova zone (up to 7.2 $M_\odot$) we consider 7 sub-zones, termed zones A-G (Table 4, Fig. 10), which we mix in variable proportions to best match the data of our X and C grains and putative nova grain N1. The considered zones extend over only 0.4 $M_\odot$, i.e., mixing occurs on comparatively small scales. This is different from the approach in the context of the Rauscher model and also from the approach applied by Xu et al. (2015) in the context of the Pignatari model r15.

As for the Rauscher model a fit is considered satisfactory if the $^{12}C/^{13}C$ and $^{14}N/^{15}N$ ratios are reproduced within a factor of two and the $^{29}Si/^{28}Si$ ratio within 10%. We relaxed the condition on $^{30}Si/^{28}Si$ because the Pignatari models use the $^{30}Si(n,\gamma)$ reaction rate from Guber et al. (2003) which is quite different from previous evaluations (e.g., Beer et al., 2002). This leaves large uncertainties on this rate which will soon be remeasured. For all X and C grains a satisfactory fit can be achieved with one of the models 25T-H20 (X2, X4, C2) and 25T-H50 (X1, X3, X5, C1) (Fig. 11). For grain X1 the predicted $^{30}Si/^{28}Si$ ratio is too high by about 50%. For the two grains for which firm ^{26}Al data exist (X1, C1) the predictions for $^{26}Al/^{27}Al$ ratios are lower than measured by factors of 7 and 17, respectively. On the other hand, the relatively low upper limit on $^{26}Al/^{27}Al$ of 0.054 in grain C2 is relatively well matched by the predicted ratio of 0.02. Inferred $^{32}Si/^{28}Si$ ratios are generally rather well matched within a factor of ~2. $^{44}Ti/^{48}Ti$ ratios in grains X1, X2, and C1 are clearly lower than predicted (by factors of 10–140). In contrast to the Rauscher model it is not possible to match $^{44}Ti/^{48}Ti$ independently by admixture of matter from a single zone, as in the Pignatari models ^{44}Ti is largely found in the Si-rich zone below the C/Si zone and adjusting the $^{44}Ti/^{48}Ti$ ratio will also affect the Si-isotopic ratios. C/O ratios are predominantly (5 out of 7 grains) larger than 1 (Table 4). Si/C is larger than 1 for the typical X grain X1 and lower than 1 (~0.2 on average) for grains with low $^{29}Si/^{30}Si$ (X2-X5) and the two C grains. This may explain, at least in part, the paucity of grains with low $^{29}Si/^{30}Si$ and of C grains compared to grains with isotopic signatures of grain X1.

The C- and Si-isotopic ratios of putative nova grains N1 and N2 can be matched by models 25T-H10 (N1) and 25T-H (N2), respectively (Fig. 12). Model 25T-H has slightly different mass limits for the C/Si and O/nova zones than the models with lower H and for the mixing we considered 6 zones instead of 7 (Table 4). For N no fit could be found; predicted $^{14}N/^{15}N$ ratios are too low for both putative nova grains by about a factor of 10 (Fig. 12). The $^{26}Al/^{27}Al$ ratio of N1 is well matched while that of N2 is lower by a factor of 16 than the prediction. The $^{32}Si/^{28}Si$ ratio of N1 is higher

Table 4
Mixing fractions (in percent of total mass in the mixture) of different SN zones in models 25T-Hx of Pignatari et al. (2015) required to best reproduce C and X grain as well as putative nova grain data.

Zone	Subzone 25T-H10/20/50	Mass ($M_\odot$)	Subzone 25T-H	Mass ($M_\odot$)	X1	X2	X3	X4	X5	C1	C2	N1	N2
Model for best fit					25T-H50	25T-H20	25T-H50	25T-H20	25T-H50	25T-H50	25T-H20	25T-H10	25T-H
Below C/Si	A	6.8000–6.8145	A	6.8000–6.8145	52.7	5.1	9.6	5.7	7.7	1.6	2.3	0.0	0.0
C/Si	B	6.8145–6.8237	B	6.8145–6.8198	0.0	5.4	7.6	9.1	9.8	0.3	7.2	2.3	7.2
	C	6.8237–6.8471			30.4	0.0	1.9	2.3	2.5	0.7	18.4	5.9	
O/Nova	D	6.8471–6.8900	C	6.8198–6.9000	5.6	5.0	3.5	4.2	4.6	33.9	33.7	10.8	21.7
	E	6.8900–6.9500	D	6.9000–6.9600	9.1	82.2	57.7	69.0	74.7	44.2	38.5	17.7	16.2
	F	6.9500–7.0026	E	6.9600–7.1637	1.0	1.7	10.0	6.7	0.3	8.3	0.0	13.3	55.0
Above O/Nova	G	7.0026–7.2000	F	7.1637–7.3000	1.3	0.6	9.8	2.9	0.4	10.9	0.0	49.9	0.0
C/O					0.29	0.93	1.12	1.06	1.20	1.68	1.54	1.58	1.06
$^{28}Si/^{12}C$					1.30	0.19	0.25	0.23	0.25	0.04	0.22	0.08	0.37

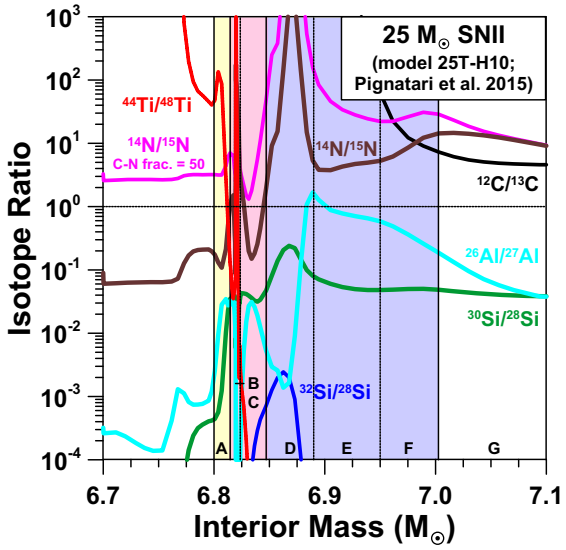

Fig. 10. Profiles of $^{12}C/^{13}C$, $^{14}N/^{15}N$ (after ^{14}C decay, with and without C-N fractionation), $^{26}Al/^{27}Al$, $^{30}Si/^{28}Si$, and $^{32}Si/^{28}Si$ in the interior of a 25 $M_\odot$ SNII according to model 25T-H10 of Pignatari et al. (2015). For fitting grain data the C/Si zone was divided into two sub-zones (B, C) and the O/nova zone into three (D–F). Two additional zones, one below the C/Si zone (A) and one above the O/nova zone (G) were considered as well. Zone A starts at 6.80 $M_\odot$ and zone G extends to 7.2 $M_\odot$.

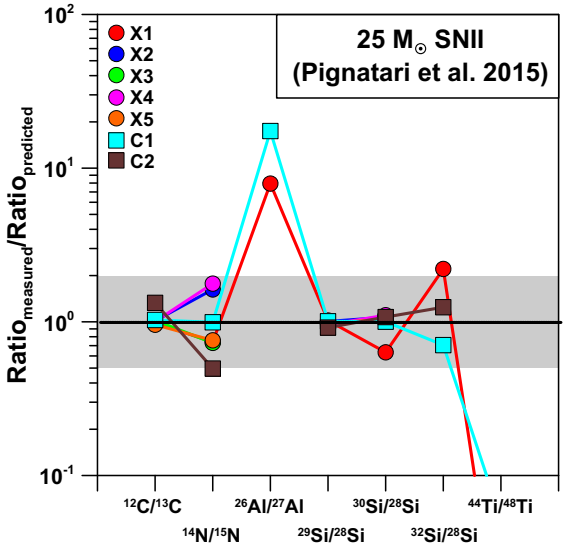

Fig. 11. Measured over predicted isotope ratios for 5 X grains and two C grains. Predictions are from model 25T-H10 of Pignatari et al. (2015) without C-N fractionation; see text for details. The gray-shaded area indicates a factor of 2 deviation of measured over predicted ratios.

by a factor of about 10 than predicted. Overall, the match of the isotope data of N1 and N2 with the model prediction is of lower quality than those for X and C grains. Since the $^{26}Al/^{27}Al$ ratio of N1 is at levels observed for SN grains, but distinctly higher than for typical nova grains, a SN origin of N1 appears a realistic possibility though (see below).

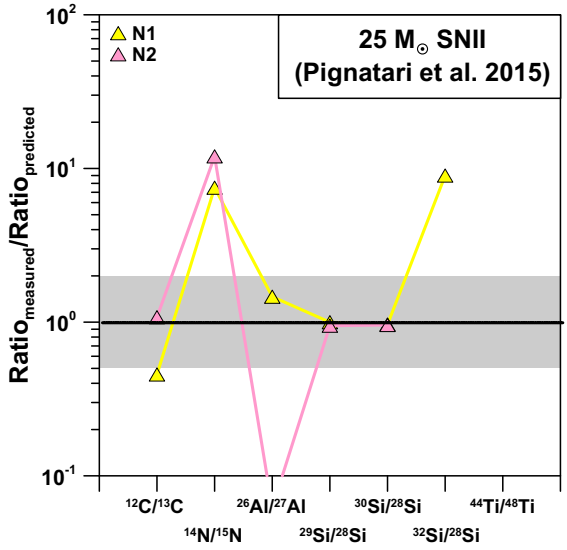

Fig. 12. Measured over predicted isotope ratios for two putative nova grains. Predictions are from model 25T-H10 of Pignatari et al. (2015) without C-N fractionation; see text for details. The gray-shaded area indicates a factor of 2 deviation of measured over predicted ratios.

The mismatch between predicted and measured $^{26}Al/^{27}Al$ ratios of X and C grains is a result of our approach to match N-isotopic ratios. If $^{26}Al/^{27}Al$ would be matched then predicted $^{14}N/^{15}N$ ratios would be too low. $^{14}N/^{15}N$ and $^{26}Al/^{27}Al$ ratios can be simultaneously matched if C-N fractionation during SiC condensation is considered. A significant fraction of ^{14}N in the SN mixtures considered here is predicted to be produced as ^{14}C and fractionated condensation of N into SiC (the time scale for dust formation is months compared to the half-life of ^{14}C of 5700 yr) would lead to higher $^{14}N/^{15}N$ ratios than predicted for unfractionated condensation (Fig. 10). We can get an estimate for the C-N fractionation from N abundances in SiC MS grains and N/C ratios in AGB stars. Models of 1.5–3 $M_\odot$ AGB stars of solar metallicity ($Z = 0.014$), the likely parent stars of MS grains, predict N/C ratios of 0.2–0.3 and only low ^{14}C abundances at the stellar surface (Cristallo et al., 2015). Nitrogen concentrations of presolar SiC grains can be estimated from measured CN^-/C^- ratios (e.g., Hoppe et al., 1994). CN^- has a much higher ion yield than C^- and relative sensitivity factors $\varepsilon(CN^-)/\varepsilon(C^-)$ between 7 and 30 have been determined for organic materials, depending on the chemical bonding between C and N (Zinner et al., 1989). We have measured CN^-/C^- on a synthetic SiC standard doped with N ($N/C = 0.131$) which yielded a relative sensitivity factor $\varepsilon(CN^-)/\varepsilon(C^-)$ of 9, well within the range determined by Zinner et al. (1989). Because the C–N bond in our synthetic SiC is likely to be different from that in presolar grains, one should be aware that significant uncertainties (at least a factor of 2) on inferred N/C ratios in presolar grains exist. Typical CN^-/C^- ratios of SiC MS grains are ~0.1 (e.g., Hoppe et al., 1994), which, with consideration of the ion yields determined on our synthetic SiC standard, corresponds to $N/C \sim 0.01$. By comparing this number with the predictions for N/C in AGB stars we obtain a C-N fractionation factor between 20 and 30 with an uncertainty of at least a factor of 2. A C-N fractionation factor of 25 is not sufficient to solve the N-Al problem but with a two times higher C-N fractionation factor of 50 (which is within the stated uncertainty) and model 25T-H10 (which produces more ^{26}Al than model 25T-H50) it is possible to simultaneously achieve a satisfactory fit for C, N, $^{29}Si/^{28}Si$, and $^{26}Al/^{27}Al$ for grains X1 and C1 (Fig. 13). The mixtures considered for these grains have $^{14}C/^{12}C$ ratios of 0.01–0.02 and since ^{14}C will be the most abundant source of ^{14}N for a C-N fractionation as considered here, N/C ratios (after ^{14}C decay) would be in the percent range as often observed for SN grains (Hoppe et al., 1996). We note that the actual C-N fractionation factor during SiC condensation in SN ejecta is not known and it remains to be seen whether detailed chemical models of SiC formation in SN ejecta can achieve C-N fractionation factors as high as 50.

Most presolar Si_3N_4 grains have $^{14}N/^{15}N$, $^{26}Al/^{27}Al$, and $^{29,30}Si/^{28}Si$ ratios similar to SiC X grains (Nittler et al., 1995; Hoppe et al., 1996; Lin et al., 2010), which suggests a related origin. It is currently not known how Si_3N_4 can form in stellar winds or ejecta. In the context of the 25T-Hx models there is no zone which shows simultaneously high Si and N concentrations (Fig. 8), which would be favorable for Si_3N_4 formation. If Si_3N_4 co-condenses with SiC from the same SN mix then one would expect lower $^{14}N/^{15}N$ ratios in Si_3N_4 grains than in SiC grains because the effect of ^{14}C decay will be suppressed. This is not observed which suggests either (i) a lower C-N fractionation during SiC condensation than proposed here or (ii) formation of Si_3N_4 from a similar but more ^{14}N-rich mix.

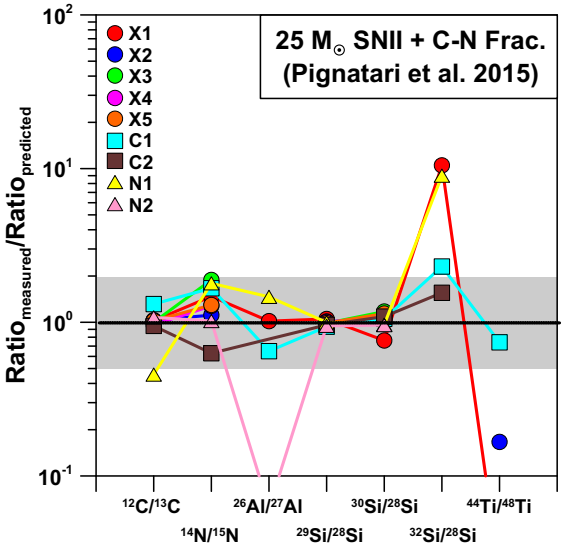

Fig. 13. Measured over predicted isotope ratios for 5 X grains, two C grains, and two putative nova grains. Predictions are from model 25T-H10 of Pignatari et al. (2015) with consideration of C-N fractionation of a factor of 50 during SiC condensation; see text for details. The gray-shaded area indicates a factor of 2 deviation of measured over predicted ratios.

Future models of dust formation in SN ejecta will hopefully address this question. If case (i) is correct, modifications to the Pignatari models are suggested, e.g., considering a different SN progenitor mass (cf. Section 4.2.1), which leads to a different pre-SN structure, or multi-dimensional hydrodynamical treatments.

If the C-N fractionation scenario is correct for grains X1 and C1 then it should also be considered for the remaining X and C grains for which no $^{26}Al/^{27}Al$ data or only upper limits exist. With models 25T-H10 (grains X2, X3, X4, X5) and 25T-H20 (grain C2) it is indeed possible to find fits that simultaneously can account for the C-, N-, and Si-isotopic compositions if C-N fractionation with a factor of 50 is considered. These fits involve matter from zones A-F which extend over only 0.2 $M_\odot$ (Table 5). For grains X2, X3, and X4 predicted $^{26}Al/^{27}Al$ ratios are 0.1–0.4, compatible with the ratios of typical X grains; for grains X5 and C2 predicted ratios are 0.1 and 0.014, respectively, compatible with the upper limits determined for these grains (Table 5, Fig. 13). Besides these positive effects on the fit quality when C-N fractionation is considered, there are also some problems that come up: For grain C2 the mixture consists almost entirely of C/Si zone matter (zones B and C; Table 5). This mixture has a $^{12}C/^{13}C$ ratio on the order of 10^7. However, we note that even small contributions of contaminating carbon to measurements of grains with very high $^{12}C/^{13}C$ ratios would lower measured ratios considerably. To get a match with the C isotope data of grain C2 requires a carbon contamination of only 4‰ which we have assumed when we plotted the C-isotopic ratio of grain C2 in Fig. 13. Except for grain C2, C/O ratios are <1 for the best fit mixtures (Table 5). Clayton et al. (1999) and Deneault et al. (2003) have suggested condensation of carbonaceous grains even while C/O < 1 in SNII ejecta. However, whether this holds for SiC has been put into doubt (Ebel and Grossman, 2001). We come back to this issue below. For $^{32}Si/^{28}Si$ ratios the fits are worse compared to the case without C-N fractionation, in particular for grain X1 for which the predictions yield about 10 times too little ^{32}Si.

As we have shown above, for putative nova grains N1 and N2 none of the Pignatari models without C-N fractionation can account for the $^{14}N/^{15}N$ ratio when matching C- and Si-isotopic ratios (Fig. 12). When we apply a C-N fractionation of a factor 50, as discussed for X and C grains, then we can match the $^{14}N/^{15}N$ ratios of N1 and N2 well (Fig. 13), even without changing the composition of the initially inferred mixtures. For N1 the only apparent larger mismatch between the grain data and model predictions would be for $^{32}Si/^{28}Si$ (Figs. 12 and 13). However, it should be noted that the error on the inferred $^{32}Si/^{28}Si$ is large (Table 2) and that the mismatch would have a significance of only 2.5σ. Overall, the isotope data of grain N1 are largely compatible with a SN origin and its high $^{26}Al/^{27}Al$ favors a SN origin over a nova origin. This view is also supported by a comparison with nova model predictions. The best matches between the isotope data of putative nova grains and model predictions are obtained when ONe nova ejecta are mixed with >95% material of close-to-solar composition (Amari et al., 2001a; José and Hernanz, 2007). The Si-isotopic signature of grain N1 favors formation in a

Table 5
Mixing fractions (in percent of total mass in the mixture) of different SN zones in models 25T-Hx of Pignatari et al. (2015) required to best reproduce C and X grain as well as putative nova grain data with consideration of C-N fractionation during condensation.

Zone	Subzone 25T-H10/20	Mass ($M_\odot$)	Subzone 25T-H	Mass ($M_\odot$)	X1	X2	X3	X4	X5	C1	C2	N1	N2
Model for best fit					25T-H10	25T-H10	25T-H10	25T-H10	25T-H10	25T-H10	25T-H20	25T-H10	25T-H
Below C/Si	A	6.8000–6.8145	A	6.8000–6.8145	13.9	3.5	7.4	3.0	7.8	0.0	4.3	0.0	0.0
C/Si	B	6.8145–6.8237	B	6.8145–6.8198	0.0	5.6	6.8	9.6	12.3	0.5	27.0	2.3	7.2
	C	6.8237–6.8471			19.5	0.0	1.97	2.5	3.1	1.2	68.7	5.9	
O/Nova	D	6.8471–6.8900	C	6.8198–6.9000	35.8	5.2	31.5	4.5	57.3	56.7	0.0	10.8	21.7
	E	6.8900–6.9500	D	6.9000–6.9600	29.2	84.6	41.1	73.2	18.7	27.7	0.0	17.7	16.2
	F	6.9500–7.0026	E	6.9600–7.1637	1.5	1.1	11.6	7.2	0.8	13.9	7.7e−5	13.3	55.0
Above O/Nova	G	7.0026–7.2000	F	7.1637–7.3000	0.0	0.0	0.0	0.0	0.0	0.0	0.0	49.9	0.0
C/O					0.44	0.63	0.64	0.81	0.81	0.64	3.16	1.58	1.06
$^{28}Si/^{12}C$					0.64	0.22	0.31	0.25	0.34	0.05	0.41	0.08	0.37

1.35 $M_\odot$ ONe nova (José et al., 2004). However, when matching the $^{12}C/^{13}C$ ratio of 3.7 in grain N1 the predicted $^{14}N/^{15}N$ ratio is <1 (Amari et al., 2001a), i.e., about two orders of magnitude lower than measured in grain N1. Carbon-14 is not expected to be involved in the nova nucleosynthesis network (Denissenkov et al., 2014) and C-N fractionation will thus not lead to an increased $^{14}N/^{15}N$ ratio.

For N2 there is a significant mismatch between measured and predicted $^{26}Al/^{27}Al$ that cannot be resolved in the context of the 25T-Hx models when matching C, N, and Si isotope data (including C-N fractionation). Given the low level of ^{26}Al in this grain compared to SiC grains of proven SN origins, a nova origin seems more favorable than a SN origin in this case. However, a comparison with nova model predictions does not support this possibility either. None of the nova models predict enrichments in ^{29}Si and ^{30}Si (José et al., 2004; Denissenkov et al., 2014); as for grain N1 the closest match with the Si isotope data of grain N2 is achieved with predictions for a 1.35 $M_\odot$ ONe nova (José et al., 2004). With respect to C and N we are experiencing the same problems as for grain N1, namely, a $^{14}N/^{15}N$ ratio that is about two orders of magnitude lower than observed. Altogether, the stellar origin of grain N2 remains enigmatic and it remains to be seen whether adjustments to the Pignatari models, e.g., by consideration of different SN progenitor masses or multi-dimensional hydrodynamics can resolve existing discrepancies between the isotope data and the model predictions.

Finally, we note that other signatures of SN grains, e.g., large ^{49}Ti excesses, which might be partially from ^{49}V decay (Hoppe and Besmehn, 2002; Lin et al., 2010), and Fe and Ni isotopic compositions could give important constraints to develop the Pignatari models further. Unfortunately, we don't have data for these isotopes for the SN grains considered here. Vanadium-49 is predicted to be produced in relatively large amounts slightly below the C/Si zone, i.e., all X grains considered here and grain C1 would be expected to show ^{49}Ti excesses from ^{49}V decay. Regarding Fe and Ni isotopes the reader is referred to the paper by Kodolányi et al. (2018).

4.2.3. Model strengths and shortcomings

If we consider only C-, N-, and Si-isotopic compositions we can find good fits to the data of SN X and C grains with the Rauscher and Pignatari models. Given the uncertainties in nuclear reaction rates and SN physics in general the quality of these matches appears remarkable. While measured $^{26}Al/^{27}Al$ ratios can be well matched by the Pignatari models, predictions are much too low in the context of the Rauscher model but can be matched if a related model of lower mass from Woosley and Heger (2007) is used. C-N fractionation and a high ^{14}C abundance are crucial for simultaneously matching $^{14}N/^{15}N$ and $^{26}Al/^{27}Al$ ratios in the context of the Pignatari models. We note that the Rauscher model also predicts lots of ^{14}C between 2.3 and 3.1 $M_\odot$. However, this region is O-rich (Fig. 6) and since contributions from this region to the mixtures considered here (Section 4.2.1) are low (Table 3) the effect of ^{14}C on the $^{14}N/^{15}N$ ratio is only small.

Predicted $^{32}Si/^{28}Si$ ratios from the Pignatari models are generally too low while for the Rauscher-Woosley-Heger models they can be too low or too high, depending on the mass of the progenitor star. For the Pignatari models 25T-Hx the underproduction of ^{32}Si is due to the fact that H ingestion into the He shell suppresses the neutron burst (see discussion in Pignatari et al., 2015). This lowers the production of ^{32}Si compared to models without H ingestion, e.g., model 15r. The too low ^{32}Si production in models 25T-Hx may be accounted for by the fact that these models are one-dimensional, while H ingestion is clearly a multi-dimensional hydrodynamical event (e.g., Herwig et al., 2014; Woodward et al., 2015). Hydrogen ingestion introduces large asymmetries in the He shell and regions with low or no H are locally favorable sites for the production of neutron-burst isotopes such as ^{32}Si which can be accounted for by multi-dimensional hydrodynamical models. A similar conclusion was drawn by Liu et al. (2016) who pointed out that SN grains with high abundances of ^{13}C and the neutron-rich Si isotopes give evidence for the independent co-existence of proton- and neutron-capture isotopic signatures which strongly supports heterogeneous H ingestion into the He shell in pre-SNe.

Measured $^{44}Ti/^{48}Ti$ ratios are well matched by the Rauscher model. As we pointed out above, the good match of $^{44}Ti/^{48}Ti$ with the predictions of the Rauscher model results from variable admixture of matter from the Ni-rich zone which does not affect other isotopic ratios. Titanium-44 is generally too high in the Pignatari models (Fig. 13). This results to a large extent from the admixture of matter from the thin Si-rich zone located directly below the C/Si zone. Some ^{44}Ti is also produced in the C/Si zone by the same α-capture chain that produces ^{28}Si (Pignatari et al., 2013a). The extension and detailed abundance profiles of the C/Si zone depend sensitively on convective boundary mixing processes below the convective He shell in the progenitor star. More simulations are needed to see how convective boundary mixing will affect ^{44}Ti abundances. This underlines the importance of presolar grains from SNe as a powerful tool to gather information about the SN shock and the structure of the progenitor star.

The Rauscher model requires deep and heterogeneous mixing, involving matter from inner and outer SN zones, extending over several $M_\odot$. While one major element, Si, originates to a large extent from the inner zones, the other major element, C, is most abundant in outer zones. Large-scale, asymmetric mixing in SN ejecta is indicated both from astronomical observations (Grefenstette et al., 2014) and multi-dimensional simulations of core-collapse SNe (Kifonidis et al., 2003, 2006; Hammer et al., 2010). Raleigh-Taylor (RT) instabilities are predicted for the Si-O and (C + O)-He composition interfaces, resulting in a clumpy ejecta (Kifonidis et al., 2003). Hammer et al. (2010) have shown in their simulation that the explosion starts already with a large-scale asphericity which is a trigger for RT instabilities resulting in deep inward mixing of H and fast-moving metal-rich clumps penetrating into the H envelope. Strong mixing of matter is predicted for the He-H composition interface along with the evolution of a strong anisotropy of the inner ejecta (Kifonidis et al.,

2006). While all this points to large-scale and intensive mixing of material in SN ejecta, it remains questionable whether full, microscopic mixing of material from very different, originally distant SN zones is possible as assumed in our mixing calculations in the context of the Rauscher model. In principle, we made a similar assumption in the context of the Pignatari models, but at much smaller scales as the matter originates within a zone of only 0.2 $M_\odot$ (all X and C grains) and 0.4 $M_\odot$ (grain N1), respectively. Another important feature of the Pignatari models is the presence of a C- and Si-rich subzone which provides much of the C and Si in the mixtures and distinctly higher Si/C ratios than for the mixtures in the context of the Rauscher models (Tables 3–5). Taken together it appears that the constraints imposed by the need for microscopic mixing are easier to fulfill in the context of the Pignatari models and that higher Si/C ratios in these models may facilitate SiC formation. The further discussion will thus focus on the Pignatari models with C-N fractionation.

As we pointed out above 6 out of the 8 best-fit mixtures for the likely SN grains have C/O < 1 (Table 5), which is unsatisfactory. Zones that are O-rich in our mixing schemes are subzone A, which is located just below the C/Si zone and provides ^{28}Si-rich matter, and much of the O/nova zone (Fig. 8). C/O ratios would be higher if subzone A would be part of the C/Si zone. E.g., if we assume a C mass fraction of 20% (as at the bottom of the C/Si zone) and no O for subzone A, then the C/O ratio of the best-fit mixture for grain X1 increases from 0.45 to 1.6. The extension and composition of the C/Si zone depends on the structure at the bottom of the convective He shell of the massive progenitor star. We will explore this in a future study in which we will investigate the relevant convective boundary mixing processes, similar to the analysis of He-burning layers in low-mass stars (Herwig et al., 2007). In any case, our mixing exercises suggest that ^{28}Si excesses are linked to C-rich material in SNe. We note, however, that the extension of the C/Si zone to lower masses will not solve the C/O ratio problem in all cases. E.g., the best-fit mixture for grain C1 contains no matter from subzone A at all, suggestive of a lower O mass fraction in the O/nova zone than currently predicted.

We note that X1 is the only grain for which the predicted ^{30}Si/^{28}Si ratio is higher (>30%) than measured. In our mixing schemes X1 contains significantly more matter from the Si-rich zone below the C/Si zone (zone A) than the other grains (Table 5). This suggests that the predicted ^{30}Si production might be too high in this layer. This supports the idea that the ^{30}Si(n, γ) reaction rate determined by Guber et al. (2003) may be indeed too low, but only under the conditions assumed for the bottom of the He burning zone. The relatively good agreement between predicted and measured ^{30}Si/^{28}Si for the remaining grains suggests that the ^{30}Si production in zones B-F, which are the main contributors to the mixtures considered here (Table 5), is well described by the models. This is in line with suggestions by Zinner et al. (2006) who favor the Guber et al. (2003) rates to account for the Si-isotopic ratios of grains that formed in low-metallicity AGB stars.

Since the C/Si zone represents essentially pure He burning products, grain C2 offers a unique opportunity to study the effects of He burning. The mixture considered here for grain C2 consists of 96% of C/Si zone matter (Table 5). The high ^{15}N and low ^{26}Al abundances of C2 confirm the predictions for He burning in the 25T-Hx models.

5. SUMMARY AND CONCLUSIONS

We report here new isotope data (C, N, Si, ^{26}Al, ^{32}S, ^{44}Ti) of six presolar SiC grains, namely, two X (named X4 and X5), two C (C1, C2), and two putative nova grains (N1, N2). Together with isotope data of three X grains from the literature (X1, X2, X3) we compare their isotope data with model predictions for different 15 $M_\odot$ SNeII (Rauscher et al., 2002; Pignatari et al., 2013a) as well as for a set of 25 $M_\odot$ SNeII with variable ingestion of H into the He burning zone (Pignatari et al., 2015). Our most important findings and conclusions can be summarized as follows:

1. Because they avoid the large-scale mixing required in the context of the Rauscher models the high-temperature 25 $M_\odot$ models of Pignatari et al. (2015), which consider H ingestion (25T-Hx) along with one-dimensional hydrodynamics, represent an important step forward in our efforts to understand X and C grain data in the context of SN models. These models, like those without H ingestion, predict a C- and Si-rich (C/Si) zone at the bottom of the He shell, an attractive site for SiC formation. Heterogeneous ingestion of H into the He shell before the explosion allows variable production of ^{13}C, ^{15}N, and ^{26}Al by explosive H burning in close proximity to the C/Si zone, so that isotopic compositions of presolar grains of potential SN origin can be matched by mixing matter originating from a region extending over only 0.2 $M_\odot$ for most grains considered here.
2. Simultaneously fitting the ^{12}C/^{13}C, ^{14}N/^{15}N, ^{29,30}Si/^{28}Si, and ^{26}Al/^{27}Al ratios of all X and C grains and one putative nova grain by the 25T-Hx models can be satisfactorily achieved if C-N fractionation by a factor of 50 is considered during SiC condensation. This leads to preferential incorporation of ^{14}C, a relatively long lived important precursor of ^{14}N, which is crucial for simultaneously matching ^{14}N/^{15}N and ^{26}Al/^{27}Al ratios. Whether detailed models of SiC formation in SN ejecta can achieve a C-N fractionation factor as high as 50 remains to be seen.
3. Silicon-isotopic ratios can generally be matched well, except the ^{30}Si/^{28}Si ratio of one X grain (representing typical X grains) which is lower by >30% than predicted. Matching its ^{12}C/^{13}C, ^{14}N/^{15}N, ^{29}Si/^{28}Si, and ^{26}Al/^{27}Al ratios requires significantly more matter from a thin Si-rich zone (0.015 $M_\odot$) below the C/Si zone than for the other grains considered here. This suggests that ^{30}Si in this Si-rich zone is lower than predicted by the model, possibly due to an erroneous ^{30}Si(n, γ) reaction rate.
4. Predictions from the 25T-Hx models for ^{32}Si are generally too low, especially for grains X1 and N1, while those for ^{44}Ti are too high when C-, N-, and Si-isotopic com-

positions and $^{26}Al/^{27}Al$ ratios are well fitted. Considering multi-dimensional instead of the currently used one-dimensional models with H ingestion may lead to a higher ^{32}Si production than currently predicted. Another problem is posed by the C/O ratios that are mostly <1 if C-N fractionation is considered. This problem could be largely relaxed (for 4 out of 6 grains) if the thin ^{28}Si- and O-rich zone below the C/Si zone, from which contributions are required to fit Si isotope ratios, would be C-rich as well, i.e., if the C/Si zone would extend to lower masses.

5. One of our putative nova grains has C-, N-, and Si-isotopic compositions and a $^{26}Al/^{27}Al$ ratio that can be well reproduced by the 25T-H10 model. This confirms previously made suggestions that at least some of the presolar grains assumed to have a nova origin might be from SNe instead.

ACKNOWLEDGEMENTS

We thank Antje Sorowka for the SEM analyses. This work was supported by DFG SPP 1385 (PH, JK) and by the Max Planck Society. MP acknowledges significant support from NSF grants PHY 02-16783 and PHY 09-22648 (Joint Institute for Nuclear Astrophysics, JINA), NSF grant PHY-1430152 (JINA Center for the Evolution of the Elements), EU MIRG-CT-2006-046520, and from SNF (Switzerland). NuGrid data are served by Canfar/CADC. MP also acknowledges PRACE, through its Distributed Extreme Computing Initiative, for resource allocations on Sisu (CSC, Finland), Archer (EPCC, UK), and Beskow (KTH, Sweden) and the support of STFC's DiRAC High Performance Computing Facilities; DiRAC is part of the National E-infrastructure. Ongoing resource allocations on the University of Hull's High Performance Computing Facility – viper – are gratefully acknowledged. We thank Reto Trappitsch, an anonymous referee, and AE Larry Nittler for constructive and helpful reviews.

REFERENCES

Alexander C. M. O. D. (1993) Presolar SiC in chondrites: how variable and how many sources? *Geochim. Cosmochim. Acta* **57**, 2869–2888.

Amari S., Anders E., Virag A. and Zinner E. (1990) Interstellar graphite in meteorites. *Nature* **345**, 238–240.

Amari S., Lewis R. S. and Anders E. (1994) Interstellar grains in meteorites: I. Isolation of SiC, graphite, and diamond; size distributions of SiC and graphite. *Geochim. Cosmochim. Acta* **58**, 459–470.

Amari S., Gao X., Nittler L. R. and Zinner E. (2001a) Presolar grains from novae. *Astrophys. J.* **551**, 1065–1072.

Amari S., Nittler L. R., Zinner E., Gallino R., Lugaro M. and Lewis R. S. (2001b) Presolar SiC grains of type Y: origin from low-metallicity asymptotic giant branch stars. *Astrophys. J.* **546**, 248–266.

Amari S., Nittler L. R., Zinner E., Lodders K. and Lewis R. S. (2001c) Presolar SiC grains of type A and B: their isotopic compositions and stellar origins. *Astrophys. J.* **559**, 463–483.

Asplund M., Lambert D. L., Kipper T., Pollacco D. and Shetrone M. D. (1999) The rapid evolution of the born-again giant Sakurai's object. *Astron. Astrophys.* **343**, 507–518.

Beer H., Sedyshev P. V., Rochow W., Rauscher T. and Mohr P. (2002) Neutron capture of ^{30}Si. *Nucl. Phys. A* **709**, 453–466.

Bernatowicz T., Fraundorf G., Ming T., Anders E., Wopenka B., Zinner E. and Fraundorf P. (1987) Evidence for interstellar SiC in the Murray carbonaceous meteorite. *Nature* **330**, 728–730.

Besmehn A. and Hoppe P. (2003) A NanoSIMS study of Si- and Ca-Ti-isotopic compositions of presolar silicon carbide grains from supernovae. *Geochim. Cosmochim. Acta* **67**, 4693–4703.

Clayton D. D., Liu W. and Dalgarno A. (1999) Condensation of carbon in radioactive supernova gas. *Science* **283**, 1290–1292.

Cristallo S., Straniero O., Piersanti L. and Gobrecht D. (2015) Evolution, nucleosynthesis, and yields of AGB stars at different metallicities. III. Intermediate-mass models, revised low-mass models, and the ph-FRUITY interface. *Astrophys. J. Suppl.* **219** (40), 21.

Croat T. K., Bernatowicz T., Amari S., Messenger S. and Stadermann F. J. (2003) Structural, chemical, and isotopic microanalytical investigations of graphite from supernovae. *Geochim. Cosmochim. Acta* **67**, 4705–4725.

Deneault E. A.-N., Clayton D. D. and Heger A. (2003) Supernova reverse shocks: SiC growth and isotopic composition. *Astrophys. J.* **594**, 312–325.

Denissenkov P. A., Truran J. W., Pignatari M., Trappitsch R., Ritter C., Herwig F., Battino U., Setoodehnia K. and Paxton B. (2014) MESA and NuGrid simulations of classical novae: CO and ONe nova nucleosynthesis. *Mon. Not. R. Astron. Soc.* **442**, 2058–2074.

Ebel D. S. and Grossman L. (2001) Condensation from supernova gas made of free atoms. *Geochim. Cosmochim. Acta* **65**, 469–477.

Fryer C. L., Belczynski K., Wiktorowicz G., Dominik M., Kalogera V. and Holz D. E. (2012) Compact remnant mass function: dependence on the explosion mechanism and metallicity. *Astrophys. J.* **749**(91), 14.

Grefenstette B. W., Harrison F. A., Boggs S. E., Reynolds S. P., Fryer C. L., Madsen K. K., Wik D. R., Zoglauer A., Ellinger C. I., Alexander D. M., An H., Barret D., Christensen F. E., Craig W. W., Forster K., Giommi P., Hailey C. J., Hornstrup A., Kaspi V. M., Kitaguchi T., Koglin J. E., Mao P. H., Miyasaka H., Mori K., Perri M., Pivovaroff M. J., Puccetti S., Rana V., Stern D., Westergaard N. J. and Zhang W. W. (2014) Asymmetries in core-collapse supernovae from maps of radioactive ^{44}Ti in CassiopeiaA. *Nature* **506**, 339–342.

Gröner E. and Hoppe P. (2006) Automated ion imaging with the NanoSims ion microprobe. *Appl. Surf. Sci.* **252**, 7148–7151.

Guber K. H., Koehler P. E., Derrien H., Valentine T. E., Leal L. C., Sayer R. O. and Rauscher T. (2003) Neutron capture reaction rates for silicon and their impact on the origin of presolar mainstream grains. *Phys. Rev. C.* **67**, 062802 (5pp).

Gyngard F., Nittler L. R. and Zinner E. (2010) Presolar SiC of Type C. *Met. Planet. Sci.* **45**, A72.

Haenecour P., Floss C., José J., Amari S., Lodders K., Jadhav M., Wang A. and Gyngard F. (2016) Coordinated analysis of two graphite grains from the CO3.0 LAP 031117 meteorite: first identification of a CO nova graphite and a presolar iron sulfide subgrain. *Astrophys. J.* **825**, 88 (9pp).

Hammer N. J., Janka H.-Th. and Müller E. (2010) Three-dimensional simulations of mixing instablities in supernova explosions. *Astrophys. J.* **714**, 1371–1385.

Herwig F., Freytag B., Fuchs T., Hansen J. P., Hueckstaedt R. M., Porter D. H., Timmes F. X. and Woodward P. R. (2007) Convective and non-convective mixing in AGB stars. *ASP Conference Series* **378**, 43–53.

Herwig F., Woodward P. R., Lin P.-H., Knox M. and Fryer C. (2014) Global non-spherical oscillations in three-dimensional 4π simulations of the H-ingestion flash. *Astrophys. J.* **792**, L3 (5pp).

Holzapfel C., Soldera F., Vollmer C., Hoppe P. and Mücklich F. (2009) TEM foil preparation of sub-micrometre sized individual grains by focused ion beam technique. *J. Microscopy* **235**, 59–66.

Hoppe P. and Besmehn A. (2002) Evidence for extinct vanadium-49 in presolar silicon carbide grains from supernovae. *Astrophys. J.* **576**, L69–L72.

Hoppe P., Amari S., Zinner E., Ireland T. and Lewis R. S. (1994) Carbon, nitrogen, magnesium, silicon and titanium isotopic compositions of single interstellar silicon carbide grains from the Murchison carbonaceous chondrite. *Astrophys. J.* **430**, 870–890.

Hoppe P., Strebel R., Eberhardt P., Amari S. and Lewis R. S. (1996) Small SiC grains and a nitride grain of circumstellar origin from the Murchison meteorite: implications for stellar evolution and nucleosynthesis. *Geochim. Cosmochim. Acta* **60**, 883–907.

Hoppe P., Annen P., Strebel R., Eberhardt P., Gallino R., Lugaro M., Amari S. and Lewis R. S. (1997) Meteoritic silicon carbide grains with unusual Si-isotopic compositions: evidence for an origin in low-mass metallicity asymptotic giant branch stars. *Astrophys. J.* **487**, L101–L104.

Hoppe P., Strebel R., Eberhardt P., Amari S. and Lewis R. S. (2000) Isotopic properties of silicon carbide X grains from the Murchison meteorite in the size range 0.5–1.5 μm. *Meteorit. Planet. Sci.* **35**, 1157–1176.

Hoppe P., Leitner J., Meyer B. S., The L.-S., Lugaro M. and Amari S. (2009) An unusual presolar silicon carbide grain from a supernova: implications for the production of silicon-29 in Type II supernovae. *Astrophys. J.* **691**, L20–L23.

Hoppe P., Leitner J., Gröner E., Marhas K. K., Meyer B. S. and Amari S. (2010) NanoSIMS studies of small presolar SiC grains: new insights into supernova nucleosynthesis, chemistry, and dust formation. *Astrophys. J.* **719**, 1370–1384.

Hoppe P., Fujiya W. and Zinner E. (2012) Sulfur molecule chemistry in supernova ejecta recorded by silicon carbide stardust. *Astrophys. J.* **745**, L26 (5pp).

Hoppe P., Cohen S. and Meibom A. (2013) NanoSIMS: technical aspects and applications in cosmochemistry and biological geochemistry. *Geostand. Geoanal. Res.* **37**, 111–154.

Huss G. R., Hutcheon I. D. and Wasserburg G. J. (1997) Isotopic systematics of presolar silicon carbide from the Orgueil (CI) carbonaceous chondrite: implications for solar system formation and stellar nucleosynthesis. *Geochim. Cosmochim. Acta* **61**, 5117–5148.

Hutcheon I. D., Huss G. R., Fahey A. J. and Wasserburg G. J. (1994) Extreme ^{26}Mg and ^{17}O enrichments in an Orgueil corundum: identification of a presolar oxide grain. *Astrophys. J.* **425**, L97–L100.

Jones S., Hirschi R., Nomoto K., Fischer T., Timmes F. X., Herwig F., Paxton B., Toki H., Suzuki T., Martínez-Pinedo G., Lam Y. H. and Bertolli M. G. (2013) Advanced burning stages and fate of 8–10 $M_\odot$ stars. *Astrophys. J.* **772**, 150 (14pp).

José J. and Hernanz M. (2007) The origin of presolar nova grains. *Meteorit. Planet. Sci.* **42**, 1135–1143.

José J., Hernanz M., Amari S., Lodders K. and Zinner E. (2004) The imprint of nova nucleosynthesis in presolar grains. *Astrophys. J.* **612**, 414–428.

Kifonidis K., Plewa T., Janka H.-Th. and Müller E. (2003) Non-spherical core collapse supernovae I. Neurtino-driven convection, Rayleigh-Taylor instabilities, and the formation and propagation of metal clumps. *Astron. Astrophys.* **408**, 621–649.

Kifonidis K., Plewa T., Scheck L., Janka H.-Th. and Müller E. (2006) Non-sperical core collapse supernovae. II. The late-time evolution of globally anisotropic neutrino-driven explosions and their implications for SN 1987 A. *Astron. Astrophys.* **453**, 661–678.

Kodolányi J., Stephan T., Trappitsch R., Hoppe P., Pignatari M., Davis A. M. and Pellin M. J. (2018) Iron and nickel isotope compositions of presolar silicon carbide grains from supernovae. *Geochim. Cosmochim. Acta* **221**, 127–144.

Lambert D. L., Gustafsson B., Eriksson K. and Hinkle K. H. (1986) The chemical composition of carbon stars. I. Carbon, nitrogen, and oxygen in 30 cool carbon stars in the galactic disk. *Astrophys. J. Suppl.* **62**, 373–425.

Lewis R. S., Tang M., Wacker J. F., Anders E. and Steel E. (1987) Interstellar diamonds in meteorites. *Nature* **326**, 160–162.

Limongi M. and Chieffi A. (2003) Evolution, explosion, and nucleosynthesis of core-collapse supernovae. *Astrophys. J.* **592**, 404–433.

Lin Y., Amari S. and Pravdivtseva O. (2002) Presolar grains from the Qingzhen (EH3) meteorite. *Astrophys. J.* **575**, 257–263.

Lin Y., Gyngard F. and Zinner E. (2010) Isotopic analysis of supernova SiC and Si_3N_4 grains from the Qingzhen (EH3) chondrite. *Astrophys. J.* **709**, 1157–1173.

Liu N., Nittler L. R., Alexander C. M. O'D., Wang J., Pignatari M., José J. and Nguyen A. (2016) Stellar origins of extremely ^{13}C- and ^{15}N-enriched presolar SiC grains: Novae or supernovae? *Astrophys. J.* **820**, 140 (14pp).

Lodders K. and Fegley, Jr., B. (1995) The origin of circumstellar silicon carbide grains found in meteorites. *Meteoritics* **30**, 661–678.

Lugaro M., Davis A. M., Gallino R., Pellin M. J., Straniero O. and Käppeler F. (2003) Isotopic compositions of strontium, zirconium, molybdenum, and barium in single presolar SiC grains and asymptotic giant branch stars. *Astrophys. J.* **593**, 486–508.

Marhas K. K., Amari S., Gyngard F., Zinner E. and Gallino R. (2008) Iron and nickel isotopic ratios in presolar SiC grains. *Astrophys. J.* **689**, 622–645.

Messenger S., Keller L. P., Stadermann F. J., Walker R. M. and Zinner E. (2003) Samples of stars beyond the solar system: silicate grains in interplanetary dust. *Science* **300**, 105–108.

Meyer B. S., Weaver T. A. and Woosley S. E. (1995) Isotope source table for a 25 $M_\odot$supernova. *Meteoritics* **30**, 325–334.

Müller B. (2016) The status of multi-dimensional core-collapse supernova models. *Publ. Astron. Soc. Aust.* **33**, e048 (29pp).

Nicolussi G. K., Davis A. M., Pellin M. J., Lewis R. S., Clayton R. N. and Amari S. (1997) S-process zirconium in presolar silicon carbide grains. *Science* **277**, 1281–1283.

Nittler L. R. (1996) *Quantitative isotopic ratio ion imaging and its application to studies of preserved stardust in meteorites* (Ph.D. thesis). Washington University, Saint Louis.

Nittler L. R. and Alexander C. M. O. D. (2003) Automated isotopic measurements of micron-sized dust: application to meteoritic silicon carbide. *Geochim. Cosmochim. Acta* **67**, 4961–4980.

Nittler L. R. and Hoppe P. (2005) Are presolar silicon carbide grains from novae actually from supernovae? *Astrophys. J.* **631**, L89–L92.

Nittler L. R., Alexander C. M. O'D., Gao X., Walker R. M. and Zinner E. K. (1994) Interstellar oxide grains from the Tieschitz ordinary chondrite. *Nature* **370**, 443–446.

Nittler L. R., Hoppe P., Alexander C. M. O'D., Amari S., Eberhardt P., Gao X., Lewis R. S., Strebel R., Walker R. M. and Zinner E. (1995) Silicon nitride from supernovae. *Astrophys. J.* **453**, L25–L28.

Nittler L. R., Amari S., Zinner E., Woosley S. E. and Lewis R. S. (1996) Extinct ^{44}Ti in presolar graphite and SiC: proof of a supernova origin. *Astrophys. J.* **462**, L31–L34.

Nittler L. R., Alexander C. M. O'D., Gallino R., Hoppe P., Nguyen A. N., Stadermann F. J. and Zinner E. K. (2008) Aluminum-, calcium- and titanium-rich oxide stardust in ordinary chondrite meteorites. *Astrophys. J.* **682**, 1450–1478.

Nomoto K., Kobayashi C. and Tominaga N. (2013) Nucleosynthesis in stars and the chemical enrichment of galaxies. *Annu. Rev. Astron. Astrophys.* **51**, 457–509.

Pignatari M., Wiescher M., Timmes F. X., Boer R. J., Thielemann F.-K., Fryer C., Heger A., Herwig F. and Hirschi R. (2013a) Production of carbon-rich presolar grains from massive stars. *Astrophys. J.* **767**, L22 (6pp).

Pignatari M., Zinner E., Bertolli M. G., Trappitsch R., Hoppe P., Rauscher T., Fryer C., Herwig F., Hirschi R., Timmes F. X. and Thielemann F.-K. (2013b) Silicon carbide grains of Type C provide evidence for the production of the unstable isotope ^{32}Si in supernovae. *Astrophys. J.* **771**, L7 (5pp).

Pignatari M., Zinner E., Hoppe P., Jordan C. J., Gibson B. K., Trappitsch R., Herwig F., Fryer C., Hirschi R. and Timmes F. X. (2015) Carbon-rich presolar grains from massive stars: subsolar ^{12}C/^{13}C and ^{14}N/^{15}N ratios and the mystery of ^{15}N. *Astrophys. J.* **808**, L43 (6pp).

Pignatari M., Herwig F., Hirschi R., Bennett M., Rockefeller G., Fryer C., Timmes F. X., Ritter C., Heger A., Jones S., Battino U., Dotter A., Trappitsch R., Diehl S., Frischknecht U., Hungerford A., Magkotsios G., Travaglio C. and Young P. (2016) NuGrid stellar data set I. Stellar yields from H to Bi for stars with metallicities Z = 0.02 and Z = 0.01. *Astrophys. J. Suppl.* **225**, 24 (54pp).

Rauscher T., Heger A., Hoffman R. D. and Woosley S. E. (2002) Nucleosynthesis in massive stars with improved nuclear and stellar physics. *Astrophys. J.* **576**, 323–348.

Stephan T., Trappitsch R., Davis A. M., Pellin M. J., Rost D., Savina M. R., Yokochi R. and Liu N. (2016) CHILI – the Chicago Instrument for Laser Ionization – a new tool for isotope measurements in cosmochemistry. *Int. J. Mass Spectrom.* **407**, 1–15.

Tang M. and Anders E. (1988) Isotopic anomalies of Ne, Xe, and C in meteorites. II. Interstellar diamond and SiC: carriers of exotic noble gases. *Geochim. Cosmochim. Acta* **52**, 1235–1244.

Travaglio C., Gallino R., Zinner E., Amari S. and Woosley S. (1998) Presolar dust grains from type II supernovae: mixing in the ejecta and silicon isotopic ratios, In *Nuclei in the Cosmos V* (ed. N. Prantzos), pp. 567–569.

Woodward P. R., Herwig F. and Lin P.-H. (2015) Hydrodynamic simulations of H entrainment at the top of He-shell flash convection. *Astrophys. J.* **798**, 49 (26 pp).

Woosley S. E. and Heger A. (2007) Nucleosynthesis and remnants in massive stars of solar metallicity. *Phys. Rep.* **442**, 269–283.

Woosley S. E. and Weaver T. A. (1995) The evolution and explosion of massive stars, II. Explosive hydrodynamics and nucleosynthesis. *Astrophys. J. Suppl.* **101**, 181–235.

Xu Y., Zinner E., Gallino R., Heger A., Pignatari M. and Lin Y. (2015) Sulfur isotopic compositions of submicrometer SiC grains from the Murchison meteorite. *Astrophys. J.* **799**, 156 (23pp).

Zega T. J., Nittler L. R., Busemann H., Hoppe P. and Stroud R. M. (2007) Coordinated isotopic and mineralogic analyses of planetary materials enabled by in situ lift-out with a focused ion beam scanning electron microscope. *Meteorit. Planet. Sci.* **42**, 1373–1386.

Zinner E. (2014) Presolar Grains. In *Meteorites and Cosmochemical Processes* (ed. A. M. Davis). Elsevier, Amsterdam, pp. 181–213.

Zinner E., Tang M. and Anders E. (1989) Interstellar SiC in the Murchison and Murray meteorites: isotopic composition of Ne, Xe, Si, C, and N. *Geochim. Cosmochim. Acta* **53**, 3273–3290.

Zinner E., Nittler L. R., Gallino R., Karakas A. I., Lugaro M., Straniero O. and Lattanzio J. C. (2006) Silicon and carbon isotopic ratios in AGB stars: SiC grain data, models, and the galactic evolution of the Si isotopes. *Astrophys. J.* **650**, 350–373.

Zinner E., Amari S., Guinness R., Jennings C., Mertz A. F., Nguyen A. N., Gallino R., Hoppe P., Lugaro M., Nittler L. R. and Lewis R. S. (2007) NanoSIMS isotopic analysis of small presolar grains: search for Si_3N_4 grains from AGB stars and Al and Ti isotopic compositions of rare presolar SiC grains. *Geochim. Cosmochim. Acta* **71**, 4786–4813.

Associate editor: Larry R. Nittler